LITHOS 482-483 (2024) 107677

Contents lists available at ScienceDirect

LITHOS

journal homepage: www.elsevier.com/locate/lithos

Timing and origin of the post-collisional Venda Nova and Várzea Alegre Plutons from the Araçuaí belt, Espírito Santo, Brazil

Clara Talca Onken [a,1,*], Jessica Eberhard-Schmid [a], Livia Hauser [a], Simone Marioni [a], Andrea Galli [a], Valdecir de Assis Janasi [b], Max W. Schmidt [a]

[a] Department of Earth Sciences, ETH, 8092 Zürich, Switzerland
[b] Instituto de Geociências, Universidade de São Paulo, CEP 05508-080 São Paulo, Brazil

ARTICLE INFO

Keywords:
Post-collisional
Araçuaí belt
Alkaline
Charnockites
U-Pb geochronology
Zircon Lu-Hf

ABSTRACT

The Venda Nova and Várzea Alegre Plutons in southeastern Brazil are post-collisional complexes formed during the gravitational collapse of the Araçuaí-Ribeira orogenic system during amalgamation of SW Gondwana. This study focuses on the petrological, geochemical, geochronological and zircon Lu-Hf isotopic signatures of both plutons to constrain and complete their ages and to characterize mantle *vs.* crustal source components.

The Venda Nova Pluton is divided into an inner, mildly alkaline, and an outer, calc-alkaline domain. One diorite, three quartz syenites and two granites from the inner domain give LA-ICP-MS zircon U-Pb ages of 492–477 ± 8 Ma. The outer domain is dominated by charnockites and norites, six measured charnockites give two zircon ages of 620–606 ± 11 Ma and 500–476 ± 14 Ma, corresponding to zircon core and rim, respectively; the only norite yielding zircons gives a nominal age of 567 ± 13 Ma, which cannot be simply interpreted as emplacement age. The various intrusives from the Várzea Alegre Pluton (gabbronorites, charnockites, monzogranites, syenogranites) straddle the alkaline to calc-alkaline affinity and yield all together a uniform age of 500 ± 8 Ma. This confirms that all lithologies from the Venda Nova inner domain and Várzea Alegre Pluton belong to the post-collisional G5 suite of this region. The Venda Nova outer domain charnockites, fit age-wise into the pre-collisional arc-related magmatism (G1 suite). The zircon rim ages obtained on these charnockites represent minor fluid-assisted partial remelting and resetting of the U-Pb system during the emplacement of the inner domain. Individual norite zircons show ages ranging from the charnockite intrusion age to the metamorphic thermal peak in this region. The Lu-Hf isotopes measured on the dated zircon crystals, yield mantle values for the charnockites from the Venda Nova outer domain (εHf: 3.4 ± 1.2 to 6.8 ± 1.5), indicating an isotopically depleted mantle source, consistent with arc magmatism. Instead, the Venda Nova inner domain and the Várzea Alegre Pluton have relatively radiogenic values (εHf: −12.3 ± 1.5 to −8.8 ± 2.9 and − 11.1 ± 1.1 to −7.4 ± 1.3, respectively) and show no significant variation between all lithologies, indicating a source dominated by a previously crustally enriched mantle with only minor crustal assimilation occurring during magma emplacement. Interestingly, the charnockite rim of Venda Nova is 100 Ma older than the inner (mildly alkaline) post-orogenic domain and belongs to the pre-orogenic calc-alkaline arc suite, while the charnockite ring at Várzea Alegre is part of the intrusion, both in time and geochemistry, and shows no increased crustal signature with respect to the rest of the pluton.

1. Introduction

Alkaline magmas can provide crucial information about the chemistry of the mantle (Balashov and Glaznev, 2006) and although they are volumetrically minor compared to other magmatic suites, they appear in all tectonic settings (Sørensen, 1974). This study focuses on mildly alkaline post-collisional magmatism, commonly associated with the gravitational collapse of orogens, when extension and lithospheric thinning lead to lithospheric mantle upwelling and reactivation (Liegeois et al., 1998). The associated decompression may produce characteristically mildly alkaline magmas, which are believed to derive from small degree partial melting of a metasomatically modified mantle

* Corresponding author.
E-mail address: clara.onken@erdw.ethz.ch (C.T. Onken).
[1] Postal address: Sonneggstrasse 5, ETH, 8092 Zürich, Switzerland.

https://doi.org/10.1016/j.lithos.2024.107677
Received 18 December 2023; Received in revised form 30 May 2024; Accepted 30 May 2024
Available online 4 June 2024

source (Pilet et al., 2008).

Mantle metasomatism mostly refers to a process where the mantle becomes enriched in incompatible elements such as large-ion lithophile elements (LILE; *e.g.* in Rb, Ba, Sr, K) and light REE (Roden and Murthy, 1985). The formation of such enriched mantle domains is a consequence of (a) fluxing with fluids and/or melts arising from subducting crustal material transferred into the mantle wedge (*e.g.* Willbold and Stracke, 2010; *source contamination* of Cornet et al., 2022), (b) lithospheric delamination (Anderson, 2005; McKenzie and O'Nions, 1983), or (c) reactive percolation of uprising asthenospheric melts interacting with the lithospheric mantle (Pilet et al., 2005; Rampone et al., 2020). These processes may lead to textural, compositional, and isotopic heterogeneities in the mantle. Such heterogeneities will then be fingerprinted in the resulting melts in case of mantle reactivation and will be directly sampled when the melts rise and evolve in a closed system. An even more complex chemical and isotopic situation is expected in an open system, when uprising melts interact with the crust during magma ascent and emplacement (*path contamination* of Cornet et al., 2022).

The degree of alkalinity of post-collisional melts mostly depends on the composition of the primitive melt, which in turn depends on source composition, especially CO_2 concentration, and degree of melting (Landoll, 1994). In a closed system, moderately alkaline primitive melts evolve to the vicinity of the alkali feldspar thermal divide, from which magma with slightly different degrees of alkalinity may evolve either to the phonolite- or to the granite-minimum (*e.g.* Upton and Thomas, 1980). In an open system, assimilation of quartzo-feldspatic crustal material would shift the melt evolution towards Si-enriched compositions and to the Si-rich side of the feldspar thermal divide. In this

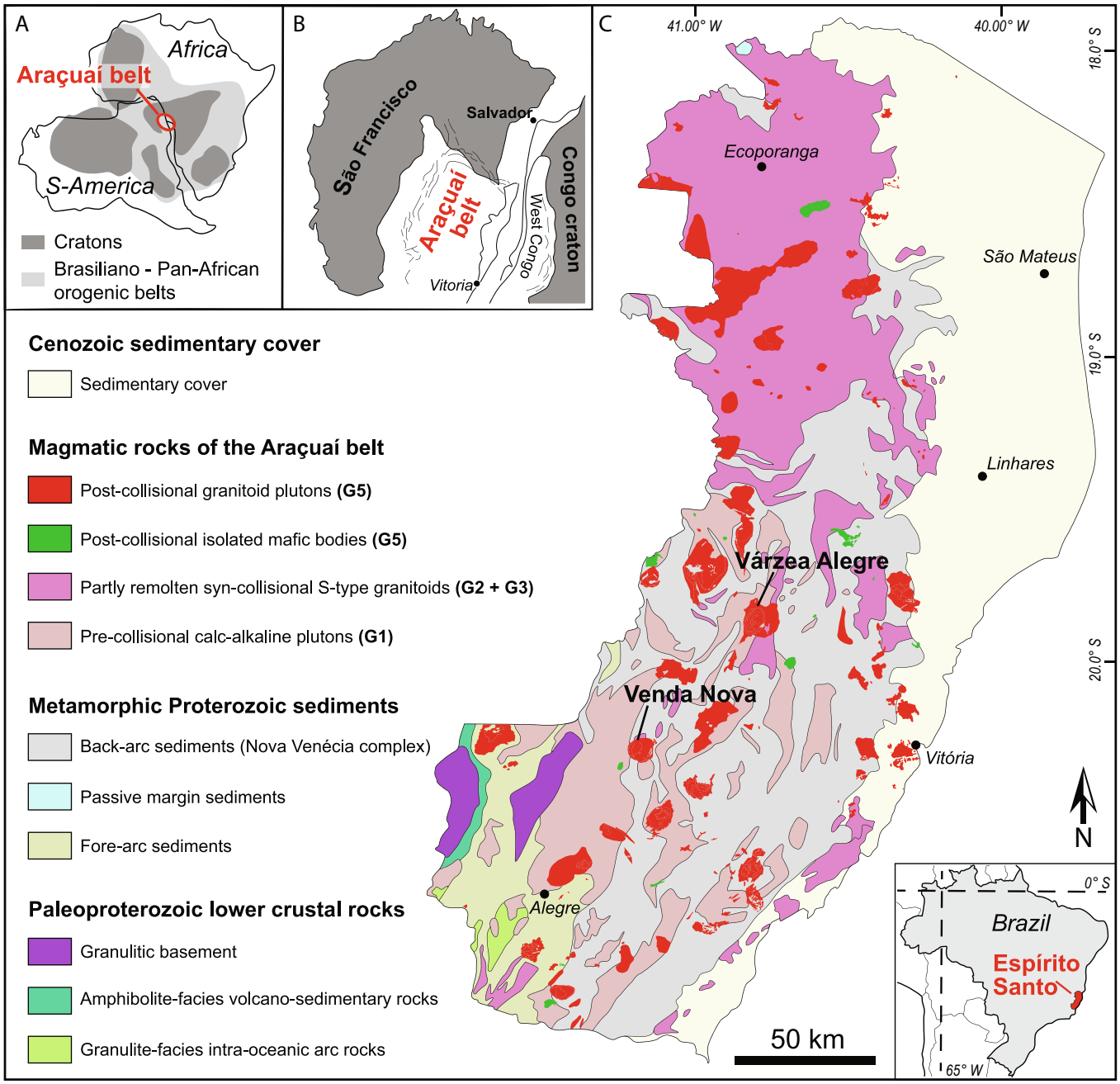

Fig. 1. A – Geotectonic setting showing the Brasiliano-Pan-African orogenic system and cratons (after Alkmim et al., 2006). B – Enlarged geotectonic view of the Araçuaí belt between the São Francisco and West Congo cratons (after Pedrosa-Soares et al., 2011). C – Geological map of the state of Espírito Santo and location of the Venda Nova and Várzea Alegre Plutons (after Vieira et al., 2018).

scenario, mildly alkaline parental melts would shift and evolve towards the granite minimum. These processes contrast the more strongly alkaline and typically Si-undersaturated basanitic parent melts that arise from deeper plumes. These mostly evolve towards the phonolite minimum, resulting in silica-undersaturated magma suites (Schairer and Bowen, 1935) that ultimately may produce carbonatitic melts, if the carbonatite-silicate miscibility gap is reached (Schmidt and Weidendorfer, 2018).

In the Araçuaí belt (SE Brazil), *ca.* 50 post-collisional plutons of Cambrian age occur. These plutons intruded in a narrow time span (520–480 Ma) but display different liquid lines of descent, allowing investigation into what governs the production and evolution of these post-collisional magmas. This study focuses on the Venda Nova and the Várzea Alegre Plutons. We present petrological, geochemical, geochronological, and zircon Lu-Hf isotopic data to understand the timing and genesis of these mildly alkaline post-collisional magma suites. With the coupled information of zircon U-Pb and Lu-Hf isotopes we constrain mantle and crustal contribution to the pre- and post-collisional magmatic systems.

2. Geological setting

2.1. The Araçuaí belt

The Araçuaí belt is part of the Neoproterozoic/early Cambrian 500 km wide and over 1000 km long Araçuaí-Ribeira orogenic system, which developed upon the closure of the Adamastor ocean, an embayment between the SE and SW margins of the São Francisco and Congo cratons in Brazil and Africa, respectively (Fig. 1). Collision between these cratons (and other continental slices) led to the formation of the Brasiliano/Pan-African orogen, producing vast amounts of orogenic and post-orogenic granitic magmatism and high-grade metamorphism ultimately shaping the SW part of Gondwana (Alkmim et al., 2006; Neves and Cordani, 1991; Pedrosa-Soares et al., 2001, 2008).

The Araçuaí belt was likely a confined orogen, where extensive magmatism was caused by the subduction of oceanic lithosphere and arc-continent collision (Amaral et al., 2020; Pedrosa-Soares et al., 2001, 2008). Another model, however, postulates that the orogen had a hot internal zone in an intracontinental setting that triggered partial melting and various magmatic products (Cavalcante et al., 2019; Fossen et al., 2017; Vauchez et al., 2007).

Magmatism in this belt is divided into five supersuites, G1 to G5. Each is related to a specific tectonic process with timespans that may regionally slightly differ, overlap between supersuites, some supersuites are composed of various magmatic pulses (*e.g.* Pedrosa-Soares et al., 2001, 2011). The G1 suite (630–575 Ma) is constituted by metaluminous, high-K, I-type calc-alkaline rocks that are now amphibolite to lower granulite facies gneisses that constitute the now exposed roots of a magmatic arc. This voluminous magmatism corresponds to the pre-collisional stage when the Adamastor ocean was subducted eastwards. The G2 suite (580–545 Ma) are mostly peraluminous S-type granitic rocks with crustal geochemical signatures formed in a *syn*-collisional context, possibly driven by a hot back-arc zone. The granitic G3 suite (545–530 Ma) was likely produced by locally remelting of G2-granites in a late syn-collisional context. The G4 suite (530–500 Ma) belongs to the same stage of crustal remelting, but is post-deformational. The G4 suite are hence early post-collisional peraluminous S-type granites, primarily found in the north of the orogen. Both G3 and G4 are minor in volume. The G5 suite then represents the late-stage post-collisional magmatism (520–480 Ma), with metaluminous to slightly peraluminous high-K alkaline suites, found along the entire belt (Fig. 1). These G5 bodies often constitute zoned magmatic bodies with mafic to intermediate cores and more felsic outer rims with local evidence of intermingling and mixing features (De Campos et al., 2004, 2016; Wiedemann et al., 2002). Geobarometric calculations yield an emplacement depth of ~10 km for the northern intrusions (2.4–3.5 kbar, Serrano et al., 2018), while the southern ones have exposure levels of 21–27 km (5.5–7.0 kbar, Mendes and De Campos, 2012). De Campos et al. (2004, 2016) interpreted the G5 complexes as the interaction of mantle-derived magmas with partial melts of the lower crust. Mechanisms postulated for triggering the post-collisional magmatism are: (a) break-off of the subducted lithospheric slab (*e.g.* Valeriano et al., 2016), (b) delamination of overthickened crust (Heilbron and Machado, 2003; Pedrosa-Soares et al., 2008) or (c) a hotspot formed after the orogenic collapse that led to the instability of the asthenospheric mantle (*e.g.* De Campos et al., 2016).

2.2. Venda Nova Pluton

The 75 km^2 large Venda Nova Pluton is located in the state of Espírito Santo (Brazil, Fig. 2), NW of Venda Nova do Imigrante. The pluton was emplaced into orthogneisses mainly belonging to the G1 suite (Estrela granitoid, leucogneiss, Santa Tereza orthogneiss; Töpfner, 1987), pre-collisional paragneisses of volcanosedimentary origin (Italva Group) and sillimanite-bearing quarzitic gneisses interpreted as the back-arc basin filling (Nova Venécia Complex; Gradim et al., 2014).

The Venda Nova Pluton is inversely zoned and exhibits a circular structure. Based on rock type and confirmed by age, the pluton is subdivided into an inner and outer domain. The inner domain consists of (i) an off-center gabbroic to dioritic core with local olivine-pyroxene-cumulates surrounded and in part gradually transitioning into monzodiorites, (ii) the dominant quartz syenites (described as "syenomonzonites" in (Ludka et al., 1998)), which are mined as dimension stones in several large quarries and which are of extraordinary homogeneity even on a 100 m scale, and (iii) several peripheral granites mainly located in the NE to SE of the pluton (Ludka et al., 1998). In the literature, the granites are not assigned to any domain, however, our geochronology shows they are contemporaneous with the inner domain (see Section 4.3). Two granite types are distinguished (Horn and Weber-Diefenbach, 1987), a coarse-grained titanite- ± microcline granite and a fine-grained leucogranite. Despite poor outcrop exposure due to dense vegetation, contacts between inner domain lithologies appear mostly gradational or lobate suggesting *syn*-magmatic intrusions. Our observations are consistent with the previous characterization as ductile and gradational contacts (De Campos et al., 2016; Ludka et al., 1998). Microgranular enclaves, xenocrysts, and pillow-like structures at the gabbronorite and quartz syenite contact is believed to indicate mingling processes (Mendes and De Campos, 2012), which is supported by geochemical data (Ludka et al., 1998).

From the NW to the S, an outer domain englobes the above inner domain with a 10 km^2 large, up to ~1 km wide, half-ring of charnockites with abundant norites to gabbronorites in the NW (Mendes et al., 2002; Mendes and De Campos, 2012). Locally, a mingling/mixing zone and also a unit of fayalite-hedenbergite syenite, dispersed but scarcely outcropping, are found in the NE and E of the pluton. The outer and inner domain contact is poorly outcropping (Mendes and De Campos, 2012). Yet, interlayered textures (schlieren) between the quartz syenites and charnockites were thought to suggest a density contrast (De Campos et al., 2004). De Campos et al. (2016) described the outer and inner domain contact as gradational, indicating coeval emplacement, but as will be seen in Section 4.3, our geochronological results, and those from Bellon et al. (2022), contradict this interpretation. Further, a few up to 20 m large schollen of charnockite were found in the quartz syenite body.

Previous studies on the Venda Nova Pluton defined the inner domain of this pluton as alkaline and K-rich, strongly enriched in Ba, Sr and LREE, but depleted in HFSE and HREE (De Campos et al., 2016). The more mafic lithologies also show a depletion in Rb and K (Ludka et al., 1998). The metaluminous and Ca-Fe-Al-enriched outer domain is tholeiitic to calc-alkaline for the norites and charnockites, respectively (Mendes et al., 2002; Mendes and De Campos, 2012). Rb-Sr and Sm-Nd isotopic analyses on an alkali gabbro from the inner domain and a

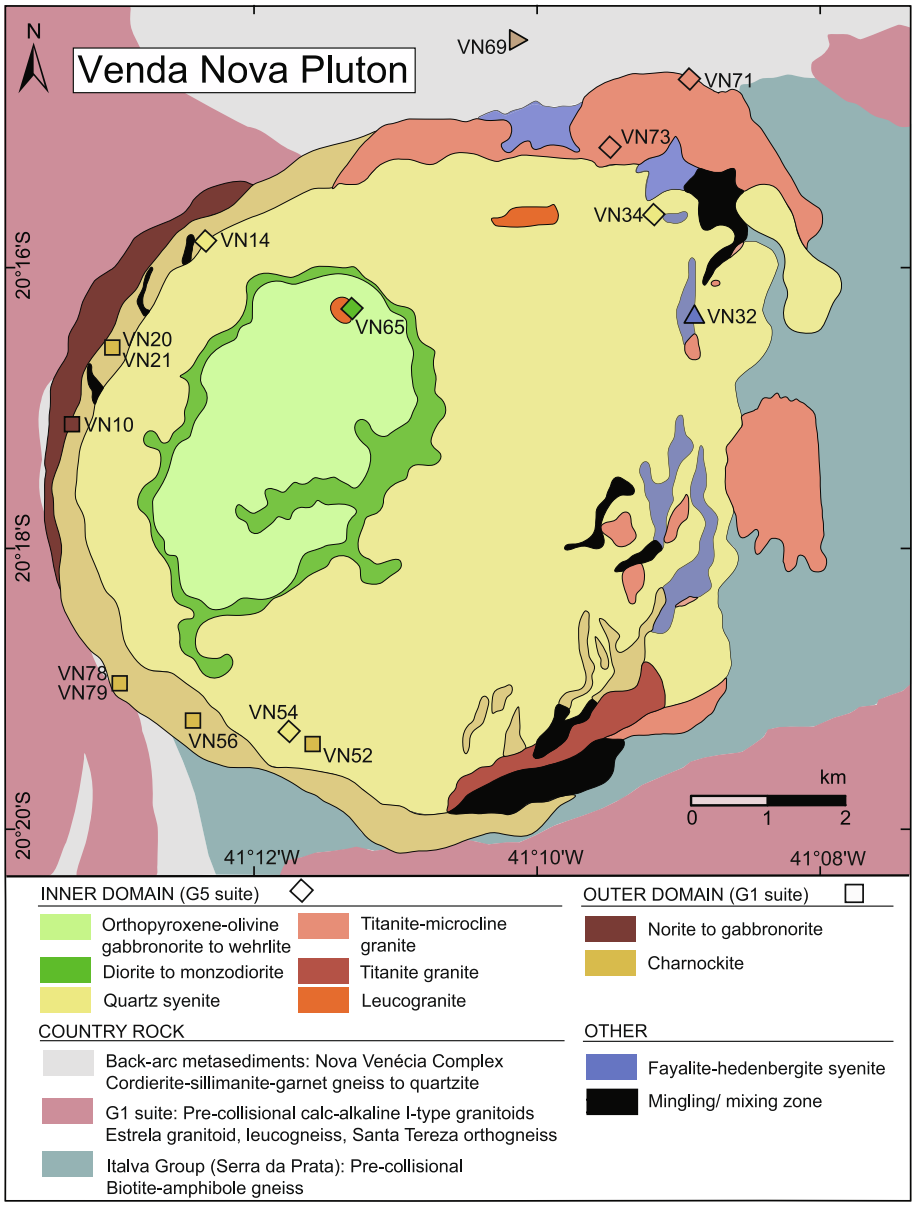

Fig. 2. Geological map of the Venda Nova Pluton modified after Töpfner (1987). Locations of the dated samples are given in diamonds for the inner domain and in squares for the outer domain. VN52 is a large (500 m) scholle in the inner domain syenite. Coordinates can be found in the supplementary material A.

charnockite from the outer domain suggest an enriched primitive mantle source for both domains (De Campos et al., 2016; Ludka et al., 1998).

Bellon et al. (2022) recently dated zircons in the quartz syenite, gabbronorite and charnockite by SHRIMP. They obtained a crystallization age of 496.9 ± 4.2 Ma for the quartz syenite and 500.6 ± 3.7 Ma for the gabbronorite. For the charnockite, they obtained two age populations in their sample: 624.0 ± 3.1 Ma as the crystallization age, and 483.7 ± 7.4 Ma representing brighter zircon rims and cores, interpreted as thermal resetting during the emplacement of the inner domain. With these ages, the observation that the charnockite geochemical signature differs from the inner lithologies, and a higher magnetic anisotropy and evidence of sub-solidus deformation features in the outer ring, Bellon et al. (2022) conclude that the charnockites belong to the pre-collisional magmatic period.

2.3. *Várzea Alegre Pluton*

The 150 km^2 large Várzea Alegre Pluton is located about 60 km NE from the Venda Nova Pluton, in proximity to Alto Santa Maria. The pluton intruded into pre- and *syn*-collisional granulitic orthogneisses (G1 and G2 undifferentiated), cordierite-sillimanite-biotite-garnet gneisses to garnet gneisses (Nova Venécia Complex; Gradim et al., 2014).

The Várzea Alegre Pluton is nearly circular and presents an inversely zoned structure (Fig. 3). It consists of, in its inner part, gabbronorites that envelop a small body of magnetite-hematite gneisses, then a hybrid zone mainly composed of quartz diorites and quartz monzodiorites with diffuse contacts, resulting from mixing and mingling of at least two magma types (Mendes et al., 2005). The middle part further has a unit of monzogranites and a small body of syenogranites (described as "megaporphyritic granites" in Medeiros et al., 2001). These inner lithologies are surrounded by a 0.5–5 km thick outer ring of porphyritic charnockites, featuring, when observed, ductile and intermingled contact relationships with the inner lithologies (Mendes et al., 2005) and a distinct foliation at the contact with the country rocks.

Geochemically, the rocks from this pluton are medium-K calc-alkaline rocks with negative εNd values and high $^{87}Sr/^{86}Sr$ ratios indicative of a strong crustal component in the magmatic source (Mendes et al.,

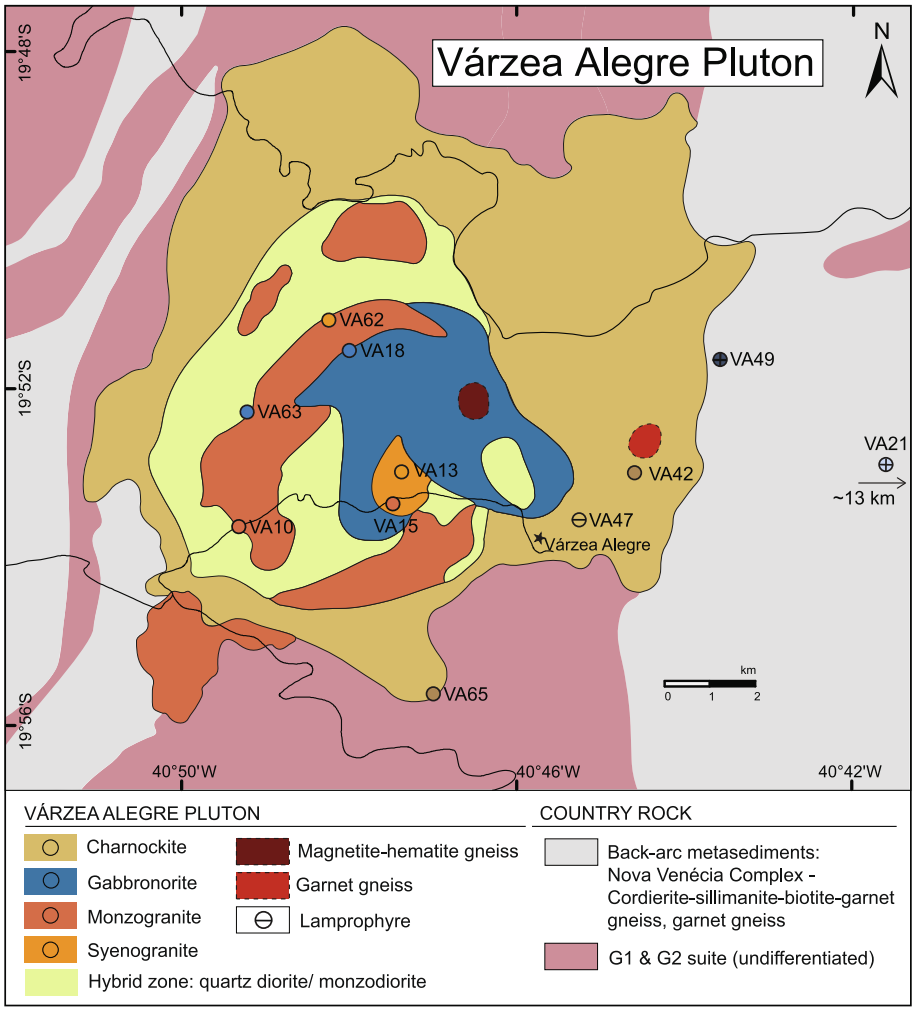

Fig. 3. Geological map of the Várzea Alegre Pluton modified after Medeiros et al. (2000) and Mendes et al. (2005). Locations of the dated samples are given in circles. Coordinates can be found in the supplementary material A.

2005). Initially, it was believed that the charnockitic unit of the Várzea Alegre Pluton was not coeval and represented a magmatic pulse different from the inner lithotypes of the pluton (Medeiros et al., 2000). Mendes et al. (2005) dated one charnockite by zircon U-Pb to 499 ± 5 Ma, in good agreement with the 508 ± 12 Ma Rb-Sr whole-rock isochron of a megaporphyric granite by Medeiros et al. (2000), yielding a coeval emplacement of the granite and charnockites.

2.4. Charnockite genesis

Charnockites *sensu lato (s.l.)* are orthopyroxene-bearing granitoids, *i.e.,* evolved with respect to mantle melts but not hydrous enough to crystallize amphibole as the dominant mafic phase (Frost et al., 2000). One prerequisite for charnockite formation within a magmatic series is, hence, a magma evolution line that is relatively H_2O-poor, which is neither uncommon in calc-alkaline nor mildly alkaline magma suites. Because of their relatively dry nature, charnockites require comparatively high temperatures (Frost et al., 2000). Prograde charnockites in fact commonly occur in high-temperature granulite-facies metamorphic terrains (Frost and Frost, 2008; Rajesh and Santosh, 2004). On that account, some charnockites are products of fluid-absent crustal biotite dehydration melting (Frost et al., 2000), some are metamorphosed granitoids in granulite-facies (*e.g.* Newton et al., 1980). Nevertheless, a magmatic origin, where orthopyroxene (often with clinopyroxene) directly crystallizes from a cooling magma is equally common (*e.g.* Kilpatrick and Ellis, 1992; Wendlandt, 1981). Variable Sr and Nd isotopic data have been reported for various charnockites pointing either to a crustal or mantle derivation (*e.g.* Janasi, 2002), showing that no unique magmatic source accounts for charnockite formation.

Both plutons studied here have a charnockite rim. In Venda Nova, the thin charnockite rim was suggested to originate from a different parental magma than the inner domain: Mendes and De Campos (2012) proposed that the charnockites differentiated from a calc-alkaline parental magma, likely resulting from the interaction between anhydrous tholeiitic magma and deeper crustal sources. In Várzea Alegre, where the charnockite unit amounts to almost half of the outcrop area, Sr-isotopes of the charnockites were interpreted as a possible result of magma mixing of a less radiogenic mantle derived magma with a more radiogenic crustal derived magma (Mendes et al., 2005).

3. Materials and methods

Representative fresh rock samples for each lithology were collected, thin sections investigated (for images see supplementary material A), and rocks or minerals analysed at ETH Zurich. For bulk rock geochemistry, rocks were cut, crushed, and milled into fine-grained homogenous powders in an agate mill. Loss on ignition (L.O.I.) was determined at 1050 °C on the powders, which were then melted in a 1:5 ratio with lithium tetraborate ($Li_2B_4O_7$) into homogenous glass discs (at 1080 °C). Bulk-rock major and some trace elements were then determined by a PANalytical AXIOS wavelength dispersive X-ray fluorescence (XRF) spectrometer (WD-XRF, 2.4 kV), trace element analyses were completed

by laser ablation inductively coupled plasma mass spectrometry (LA-ICP-MS) on broken glass shards of the glass discs. Laser frequency was set to 10 Hz and fluence to 10 J/cm^2, primary NIST610, secondary BCR-2G reference materials were used for calibration. Reported results are the average of three spot analyses of the glass discs and data were reduced using SILLS in MATLAB (Guillong et al., 2008).

For age determinations, samples were treated by a SelFrag selective fragmentation device and then sieved to obtain the fraction <500 μm, which was subsequently processed using a Holmann Wilfley table. Under an optical microscope, zircons were handpicked from the heaviest fraction from the Wilfley table, then mounted in epoxy resin and polished to expose their longitudinal sections. Zircons were imaged using a Deben Centaurus panchromatic CL cathode equipment on a JEOL JSM-6390 LA scanning electron microscope (CL-SEM).

Zircon trace elements and U-Pb isotopes were determined by LA-ICP-MS using a Thermo Element XR SF-ICP-MS mass spectrometer equipped with a Resonetic Resolution 155 laser system, 193 nm excimer laser, and Laurin Techniques resolution 155 ablation cell. Analyses were calibrated with primary standards NIST610 for zircon trace elements and GJ-1 for zircon U-Pb, secondary reference materials AUSZ7–1, *Plešovice*, Temora2, 91,500, and a zircon blank, regularly measured between the samples (supplementary material B). The analyses were carried out by measuring 30 s background followed by 30 s ablation with a 19–25 μm beam spot size, 5 Hz pulse frequency and 2.5 J/cm^2 beam energy density. Corrections for the gas blank, downhole fractionation, drift and offset on the U-Pb and trace element data were applied using the Iolite software package (Paton et al., 2011). For further U-Pb data processing and visualization the IsoplotR software (Vermeesch, 2018) was used. Age uncertainties are given at the 2σ level and include the systematic uncertainty of the facility (1.5%). Spots that had trace element concentrations affected by inclusions with $P > 1000$ ppm, Ti > 100 ppm and Ca > 1000 ppm or showing clear hydrothermal REE patterns, as well as some concordant spots that were statistical outliers, were discarded for the age calculation. In all measured samples, several measurements were excluded from the age calculation due to the effects of common Pb and Pb-loss.

Lu-Hf isotopes of the zircons were measured by a Nu Plasma II multi-collector inductively coupled plasma mass spectrometer (MC-ICP-MS). Analyses were calibrated using MudTank, Temora, QGNG, *Plešovice*, 91,500, GJ-1, GHR1 and RAk-17 (supplementary material C). The analyses were carried out by measuring 30 s background and 60 s simultaneous measuring of Lu, Yb, and Hf isotopes, with a 50 μm beam spot size, 5 Hz pulse frequency and 4 J/cm^2 beam energy density. The beam spot was targeted on the same zircon grains as the U-Pb measurement. Initial Hf isotopic compositions were calculated using the measured $^{176}Hf/^{177}Hf$, $^{176}Lu/^{177}Hf$ ratios, the corresponding samples crystallization age, and the decay constant of Söderlund et al. (2004) for ^{176}Lu ($\lambda = 1.867 \times 10^{-11}$). εHf(t) was calculated using the CHUR parameters of Bouvier et al. (2008). Initial $^{176}Hf/^{177}Hf$ (t) ratios and the εHf(t) values are reported as the average of all measurements corrected for their concordant ages. Errors are 2-standard deviations. For consistency, the same calculation scheme was applied whenever possible to the literature data.

4. Results

4.1. Petrography of the dated samples

4.1.1. Venda Nova inner domain

The *diorite* (VN65; from the opx-olivine gabbro unit) is fine- to medium-grained with an inequigranular to porphyritic texture mostly of feldspar and clinopyroxene phenocrysts. Plagioclase has simple and polysynthetic twinning. The finer-grained matrix contains feldspars, biotite, quartz and rounded clinopyroxene and orthopyroxene (cpx:opx >1, opx 5–10 modal%). Replacement textures of clinopyroxenes with orthopyroxene rims and *vice-versa* are common. Accessory phases include apatite, zircon, amphibole and Fe-Ti-oxides, often included in the silicates and surrounding the pyroxenes.

The *quartz syenites* (VN14,34,54; from the quartz syenite unit) are coarse-grained with porphyritic textures made of up to 2–5 cm large feldspar crystals. Alkali feldspar occurs with perthitic and cross-hatched microcline twinning, plagioclase with polysynthetic twinning. Other phases include green pleochroic amphibole with sub-anhedral grain shapes that form clusters with biotite, Fe-Ti-oxides and accessory phases. Quartz forms commonly myrmekitic textures along feldspar grain boundaries. Accessory phases are abundant and include eu- to subhedral apatite, titanite and zircon. Titanite is mostly associated with the Fe-Ti-oxides. The samples have variable degrees of sericitic alteration.

The most common granite *sensu stricto (s.s.)* type is a *titanite-microcline granite* (VN71,73; from the equivalent granite unit), which consists of inequigranular medium- to coarse-grained and predominantly alkali feldspar, plagioclase and quartz. The alkali feldspar megacrysts (up to 1 cm) have perthitic exsolution and cross-hatched twinning. Plagioclase occurs mostly interstitial with polysynthetic twinning, quartz exhibits myrmekitic textures. Less abundant biotite and green amphibole appear only as embayed grains. Up to 1 mm large sub-anhedral titanite crystals are ubiquitous, some show replacement by Fe-Ti-oxides. Zircon, apatite and minerals of the epidote supergroup (*e.g.* allanite) can be identified.

4.1.2. Venda Nova outer domain

The *norite* (VN10; from the norite-gabbronorite unit) shows an inequigranular-polygonal texture and is fine- to medium-grained. It is hornblende- and orthopyroxene-rich. Amphiboles are mostly subhedral with strong green to brown pleochroism, often forming reaction rims around the anhedral orthopyroxenes (opx:cpx >1, opx 10–25 modal%). Plagioclase occurs as equigranular subhedral grains with polysynthetic twinning and form polygonal aggregates. Clinopyroxene, biotite, apatite, zircon and Fe-Ti-oxides are present in minor proportions.

The *charnockites, i.e.,* opx-bearing granitoids (VN20,21,56,78,79; from the charnockite unit; VN52 is a large (500 m) scholle in the inner domain quartz syenite.) are medium- to coarse-grained with inequigranular textures composed of orthopyroxene, plagioclase, quartz, amphibole, biotite, alkali feldspar and minor clinopyroxene in some samples. Orthopyroxene is sub-anhedral and associated and in part replaced by green amphiboles, forming 2 mm sub-anhedral crystals; biotite is also closely associated with orthopyroxene and amphibole. Plagioclase with polysynthetic twinning is the dominant feldspar and either forms crystals with many inclusions and sericitic alteration or smaller pristine crystals. Quartz is present in all samples, sometimes with myrmekitic textures. Accessories are apatite, zircons, titanite and Fe-Ti-oxides.

4.1.3. Venda Nova – others

A *fayalite-hedenbergite syenite* (VN32) was observed in an isolated poor outcrop in the NE of the intrusion. To our knowledge, this rock type has not been described yet in Venda Nova. The texture of the syenite is equigranular-hypidiomorphic and medium-grained, it is dominated by alkali feldspar, hedenbergitic clinopyroxene and accessory fayalitic olivine. The alkali feldspars (up to 2 mm) show perthitic exsolutions. The hedenbergite is sub-anhedral and also shows fine exsolution lamellae. The fayalite is rounded and many crystals were completely altered to iddingsite, a reddish-brown replacement aggregate after olivine. Hornblende, Fe-Ti-oxides and zircons are present in minor proportions. An explanation for the fayalite is easily found, as at crustal pressures very low X_{Mg}-orthopyroxene destabilizes to fayalite+quartz (Frost and Frost, 2008; Mücke, 2003). As will be seen, the origin of these syenites remains unclear.

One country rock was dated, a *cordierite-garnet-sillimanite gneiss* (VN69) about 1 km distant from the intrusion. It is characterized by migmatitic banding of centimetric leucosomes of quartz, alkali feldspar and minor plagioclase, cordierite and garnet (up to 4 mm). The millimetric melanocratic layers are composed of biotite, acicular sillimanite,

quartz and plagioclase. As accessory minerals, zircons have pleochroic halos in biotite and cordierite; further, there is monazite, apatite and Fe-Ti-oxides.

4.1.4. Várzea Alegre

The *gabbronorite* (VA18; from the gabbronorite unit) is medium- to coarse-grained and has an equigranular, interlobate texture. It is composed of sub-anhedral clinopyroxene with occasional twinning lamellae, eu-subhedral orthopyroxene, biotite, plagioclase with polysynthetic twinning, alkali feldspar, large apatite crystals, quartz with myrmekitic textures, minor amphibole clustering with the pyroxenes, Fe-Ti-oxides, embayed titanite and zircon. The *gabbronorite* (VA63; from the hybrid zone unit) is medium-grained with an inequigranular and interlobate texture formed by plagioclase (with polysynthetic twinning), alkali feldspar, quartz, biotite with many inclusions, clinopyroxene mostly altered in the core but with pristine rims, minor orthopyroxene and quartz and accessory minerals such as apatite, zircon and Fe-Ti-oxide.

A *syenogranite* (VA62) and a *monzogranite* (VA10; both from the monzogranite unit), are medium- to coarse-grained with a massive structure and porphyritic, interlobate texture. Mineralogically, both rock types are composed of alkali feldspar megacrysts of up to 4 cm, showing some sericitic alteration, microcline crosshatching and perthitic textures. The coarse-grained matrix contains abundant quartz and biotite, plagioclase (more in VA10), accessory phases include apatite, titanite, zircon, epidote and Fe-Ti-oxides. The monzogranite has some minor xenomorphic amphibole.

The leucocratic *syeno-* (VA13) and *monzo-* (VA15) *granites* (both from the syenogranite unit) show an inequigranular, interlobate texture. The rock is fine- to medium-grained and composed of both feldspars, biotite flakes and quartz, sometimes with myrmekitic textures at the contact with feldspars. Minor embayed amphibole is present in sample VA15. Apatite, zircon and Fe-Ti-oxides are common.

The *charnockites* (VA42,65; from the charnockite unit) represent the most abundant lithology of the Várzea Alegre Pluton, surrounding all other facies. The charnockites have inequigranular, interlobate textures, are medium- to coarse-grained and composed of ortho- and clinopyroxene, megacrysts of alkali feldspar and plagioclase (2–3 cm), quartz with local myrmekitic texture, biotite, minor dispersed amphibole and accessory minerals including apatite, zircon, titanite and Fe-Ti-oxides.

A fine-grained, inequigranular *lamprophyre* (VA47) dyke intruded in the SE into the charnockitic unit. The main phases are small euhedral clinopyroxene, plagioclase often forming phenocrysts (up to 4 mm) and minor alkali feldspar, within a finer-grained matrix with additional biotite, apatite, zircon and Fe-Ti-oxides. A subtle mineral orientation is visible, probably caused by magmatic flow.

Two paragneisses in the vicinity of the pluton have also been dated. One is a *cordierite-sillimanite-biotite-garnet gneiss* (VA21) located 13 km E of the pluton; the dated part is its leucosome showing no foliation. The leucosome is composed of garnet (max. 5 mm) with numerous inclusions, sillimanite, alkali feldspar, quartz, cordierite and minor biotite. The other is a *garnet gneiss* (VA49) 400 m from the eastern contact. Besides garnet, it contains cordierite, quartz, biotite, both feldspars and zircon.

4.2. Bulk-rock geochemistry

4.2.1. Venda Nova Pluton

The samples from the inner and outer domains of Venda Nova show distinct geochemical characteristica and evolutions (Fig. 4), yet, are all metaluminous (bulk-rock compositions in supplementary material A). The diorite, quartz syenites and granites from the inner domain with 49.4–70.6 wt% SiO_2 and 5.9–10.6 wt% total alkalis, follow a mildly alkaline trend, ultimately evolving to the granite minimum. In contrast, the norite and charnockites from the outer domain, with 50.2–59.2 wt% SiO_2 and 4.3–5.5 wt% total alkalis, follow a sub-alkaline trend, also evolving towards the granite minimum; the charnockites are of calc-alkaline affinity (see MALI plot in supplementary material A). The Venda Nova inner domain is characterized by high K_2O concentrations, 2.8 wt% for the diorite, 5.7–6.7 wt% for the quartz syenites and 5.5–6.3 wt% for the granites. Instead, the Venda Nova outer domain has low K_2O of 0.8–1.5 wt%. Further, in the FeO*-silica diagram ($FeO^* = FeO^{total}/(FeO^{total} + MgO)$) the inner domain plots at the boundary between the magnesian and ferroan fields, whereas the outer domain is clearly magnesian (see FeO*-silica plot in supplementary material A).

Primitive mantle-normalized trace elements (Fig. 5A) from the inner domain show patterns almost one order of magnitude higher than the outer domain. The inner domain is significantly enriched in LILE elements such as in Rb, Ba and K, and LREE, and has pronounced negative Nb, Ta, Sr, P and Ti anomalies, mostly consistent with what has already been described (*e.g.*De Campos et al., 2016). In contrast, the outer domain has negative Nb and Ta anomalies and a slightly positive Sr-anomaly, overall patterns are much smoother than for the inner domain.

The fayalite-hedenbergite syenite is highly ferroan and alkaline (see supplementary material A), plotting close to the quartz syenites from the inner domain. It is marked by a low X_{Mg} of 0.04, stabilizing fayalite in this rock, and has 4.4 wt% K_2O and 6.8 wt% Na_2O. This Na-concentration is the highest reported for the Venda Nova Pluton, and even when olivine-bearing, this would be the most evolved magma of Venda Nova, yet trace element patterns neither fit the inner nor outer domain intrusives, its origin remaining somewhat enigmatic.

4.2.2. Várzea Alegre Pluton

The Várzea Alegre Pluton follows a sub-alkaline trend in the TAS diagram (Fig. 4), the gabbronorite to syenogranite have 48.6–70.4 wt% SiO_2 and total alkalis of 4.4–8.6 wt%. K_2O ranges from 1.7 to 6.1 wt%, similar to the Venda Nova inner domain. The gabbronorites, lamprophyres and charnockites are metaluminous while the monzo−/syenogranites become weakly peraluminous (the aluminium saturation index (ASI) remaining below 1.1). Similar to the Venda Nova inner domain, the samples straddle the magnesian-ferroan boundary and the MALI index indicates a calc-alkalic to alkali-calcic affinity (supplementary material A). Trace element patterns for the Várzea Alegre (Fig. 5B) are somewhat less enriched than those of the Venda Nova inner domain, but show the same, yet lesser pronounced anomalies in Nb, Ta, Sr, P, and Ti, rendering them akin to the Venda Nova inner domain. In general, the charnockites from the Várzea Alegre Pluton are less metaluminous, less calcic and show a lower X_{Mg}, higher K_2O, total alkali and TiO_2 than the charnockites from the Venda Nova outer domain. Instead, the charnockites from the Venda Nova outer domain are much more depleted in Rb, Ba, Zr, and LREE than the Várzea Alegre charnockites.

4.3. Zirconology and U-Pb geochronology

This section presents zircon morphology (Figs. 6, 7), trace element features, and the U-Pb ages of each analysed lithology. A summary of concordia ages, their uncertainties and statistics is presented in Table 1. Complete zircon trace element, U-Pb data and chondrite-normalized REE diagrams can be found in the supplementary material B.

4.3.1. Venda Nova inner domain

Zircons from the *diorite* are mainly short prismatic to rounded and 50–225 μm in length. The CL-images show a dominantly homogenous internal structure with occasional patchy-zoned features. Only minor zoning is identified and xenocrystic cores are absent. Zircons from the *quartz syenites* are primarily long prismatic, euhedral to subhedral and 100–500 μm in length. Almost all crystals show oscillatory growth zoning, only a few are homogenous. Some up to 75 μm large inclusions are present. *Granite* zircons are mostly euhedral and long prismatic with 115–350 μm length. Oscillatory and sector zoning documents their magmatic origin (Belousova et al., 2006), yet, some are homogenous.

Despite different degrees of differentiation, the zircon trace elements

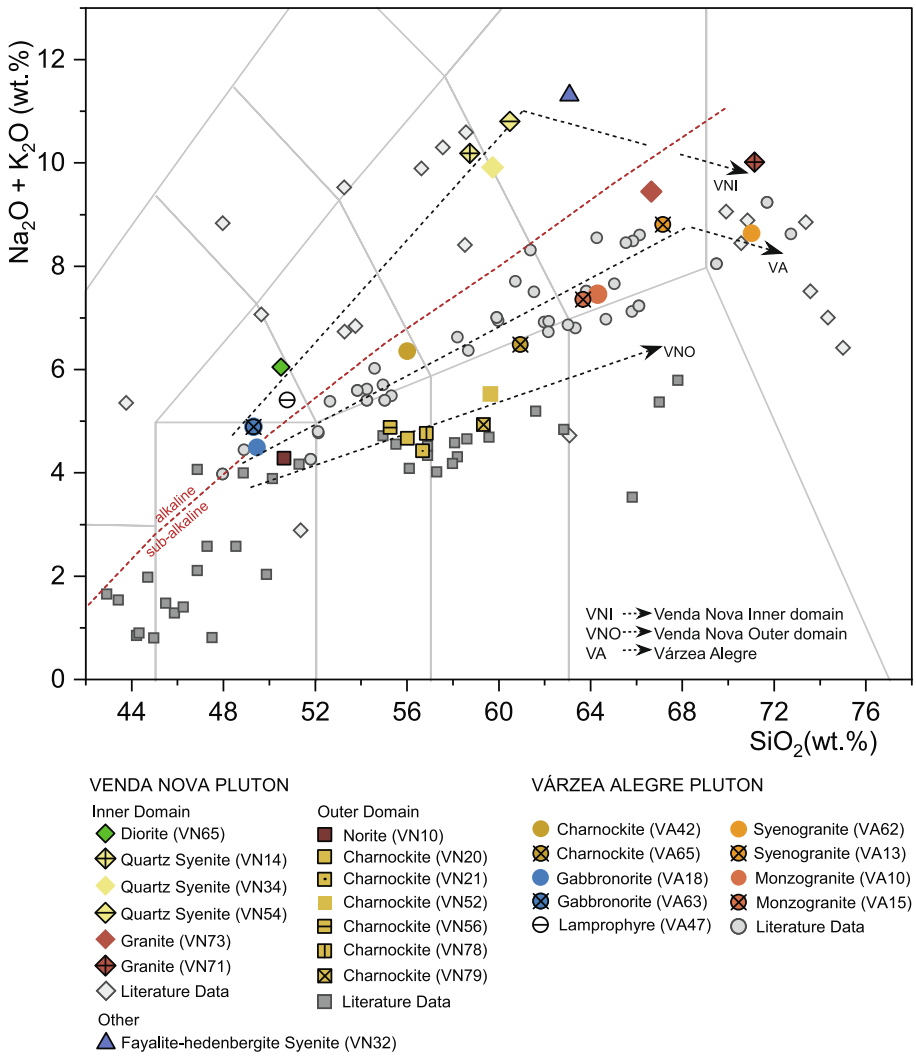

Fig. 4. Total alkalis *vs.* silica diagram (TAS, after Middlemost, 1994). The colours are the same as in the geological maps. Literature data from Ludka et al. (1998), Mendes et al. (2002) and De Campos et al. (2004) for Venda Nova and from Medeiros et al. (2000); Wiedemann et al. (2002) and Mendes et al. (2005) for Várzea Alegre.

do not significantly differ between samples. Generally, zircons of the inner domain show typical magmatic Th/U ratios, on average 1.3–2.2. Chondrite-normalized REE patterns of the concordant zircons yield enrichment in HREE and depletion in LREE, with a Lu_N/Sm_N ratios of 39–82. All have a positive Ce- and negative Eu-anomalies (Eu_N/Eu_N = 0.4–0.5), as commonly observed in magmatic zircons (Hoskin and Ireland, 2000).

The diorite (VN65) gave a concordant age of 477 ± 7.4 Ma (Fig. 8A), the different quartz syenites (VN14,34,54) 491 ± 7.5 Ma, 492 ± 7.6 Ma and 481 ± 7.5 Ma (Fig. 8B, C, D), respectively, and the two granites (VN71,73) 486 ± 7.5 Ma and 491 ± 7.6 Ma (Fig. 8E, F), respectively.

4.3.2. *Venda Nova outer domain*

Zircons in the *norite* are rounded to elongated with 40–200 μm length. Their CL-images reveal dark structureless cores, which graduate to a thin brighter rim, likely indicating a higher enrichment in trace elements. In the *charnockites*, zircons are 50–275 μm in length, either rounded or short prismatic with sub-euhedral terminations. Zircons often show dark cores and strongly luminescent unzoned rims, nevertheless, concentric oscillatory to sector zoning is identifiable in some cores (*e.g.* in VN56). Mineral inclusions of apatite, quartz and plagioclase are common.

Trace element concentrations are more variable than for zircons from the inner domain, Th/U ratios are, on average, 0.6–0.7 for the charnockites and 0.3–9.2 for the norites. HREE are enriched over LREE, with a Lu_N/Sm_N ratios of 248–312 for the charnockites and 12.1–353 for the norites. All zircons have pronounced positive Ce- and negative Eu-anomalies (Eu_N/Eu_N = 0.3–0.4 for the charnockites and 0.4–0.8 for the norite). The trace element data suggest a magmatic origin for zircons of the outer domain (Hoskin and Ireland, 2000).

The norite yields a concordant mean age of 567 ± 13 Ma (VN10; Fig. 9A), which is however, only made up by 12 concordant (out of 52, Table 1) zircon measurements which are distributed between 610 and 550 Ma. Two charnockites give a single U-Pb age of 620 ± 9.7 Ma (VN56, Fig. 9B) and 613 ± 9.9 Ma (VN21, Fig. 9C). Instead, four charnockites give two clearly distinct concordant ages: VN20 yields 609 ± 9.6 Ma for zircon cores and 482 ± 11.6 Ma for zircon rims (Fig. 9D, E); VN52 yields 606 ± 9.3 Ma and 476 ± 7.4 Ma (Fig. 9F, G). The last two charnockite samples VN78 and VN79 yield again zircon cores of 610 ± 10.9 Ma and 613 ± 9.6 Ma (Fig. 9H, J), and zircon rim ages of 498 ± 14.4 Ma and 500 ± 13.9 Ma (Fig. 9I, K), respectively. Clearly, the zircon rim ages are similar to the inner domain ages. These CL-bright rims cut the primary oscillatory zoning in the darker cores, which yield the zircon core ages, a texture different from the zircons of the inner domain. In the charnockites VN52 and VN79 some zircons are entirely luminescent, their centers also showing the younger concordant ages of ~500 Ma.

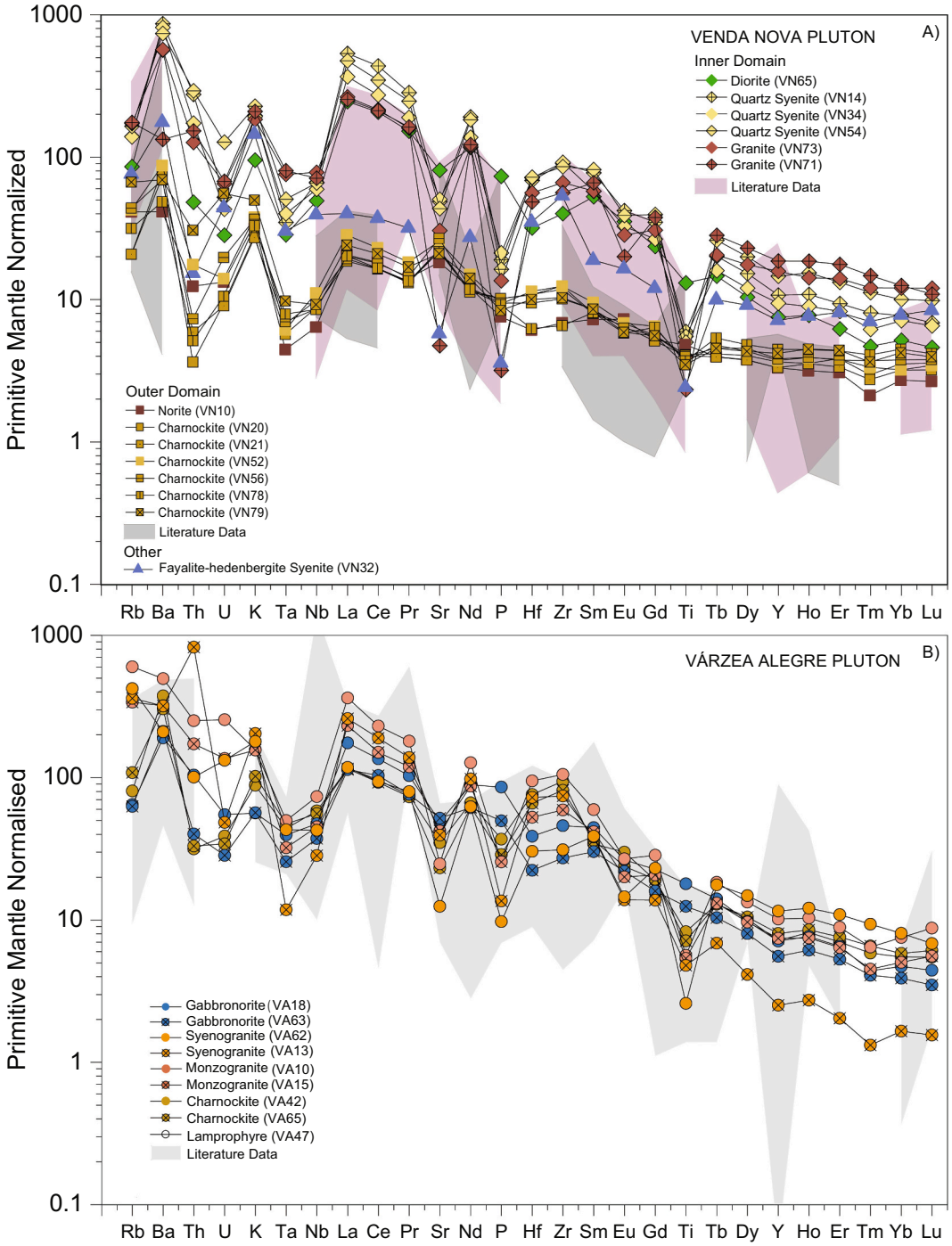

Fig. 5. Primitive mantle normalized spider diagram for A) Venda Nova and B) Várzea Alegre Pluton. Literature data given in grey shaded areas from Ludka et al. (1998) and De Campos et al. (2004) for Venda Nova inner domain, from Ludka et al. (1998) and Mendes et al. (2002) for Venda Nova outer domain and from Mendes et al. (1997), Medeiros et al. (2000), Wiedemann et al. (2002) and Mendes et al. (2005) for Várzea Alegre.

Finally, no major chemical differences, for example in the REE-patterns, are seen between zircon core and rim from the charnockites. Notably, lower Th and U concentrations are seen in the zircon rim compared to the core.

4.3.3. Venda Nova – others

In the *fayalite-hedenbergite syenite* (VN32), two zircon populations can be distinguished by their morphology. The first group is 30–100 μm in length, rounded to slightly elongated and shows dark homogenous cores grading to moderately brighter rims. The second group is constituted by subhedral prismatic zircons, 120–200 μm in length and has a characteristic oscillatory and sector zoning. The first and second zircon groups have a Lu_N/Sm_N of 15–137 and 27–266 and an Eu-anomaly of 0.4–0.8 and 0.2–0.5, respectively. Both groups have Th/U ranging from 0.2 to 2.0, with on average slightly lower Th and U concentrations in the second group. These two populations yield different concordant ages, not correlated with core-rim features. The 1st population smaller rounded zircons define an age of 624 ± 13.8 Ma (Fig. 10A) while the bigger prismatic zircons yield a younger concordant age of 488 ± 7.6 Ma (Fig. 10B), overlapping with the inner domain age.

Zircons from the *cordierite-garnet-sillimanite gneiss* (VN69) are 50–100 μm long and characterized by dark, likely detrital cores

Fig. 6. Representative zircon CL-images of the dated samples from the Venda Nova Pluton.

transitioning into oscillatory zoning with fine brighter rims. Th/U ratios are on average 0.06, very different than for the Venda Nova intrusion, but typical for metamorphic zircons (Hoskin and Ireland, 2000). Their LREE pattern is much steeper with an average Lu_N/Sm_N of 392. The zircons still show positive Ce- and negative Eu-anomalies, somewhat more pronounced (Eu_N/Eu_N = av. 0.2) than in the intrusion. U-Pb ages range between 570 and 542 Ma with a concordant age of 556 ± 9.8 Ma (Fig. 10C). This age includes core and rim measurements, as the few measured crystals did not show an age progression between core and rim, *i.e.,* did not cluster into two different age populations.

4.3.4. *Várzea Alegre*

The *gabbronorite* (VA18) has homogeneous either prismatic zircons reaching 450 µm in length or small and rounded ones that reach only 50 µm. Zircons in the other *gabbronorite* (VA63) are 50–250 µm in size and mostly euhedral with brighter rims often showing more apparent zonation patterns than cores. Inclusions of up to 25 µm are sometimes present. Zircons from the *monzogranite* (VA10) and *syenogranite* (VA62) are similar, 100–200 µm in length, idiomorphic and prismatic with oscillatory zoned rims and mostly homogeneous cores. The *syenogranite* (VA13) and *monzogranite* (VA15) have 30–200 µm long zircons, typically euhedral and long prismatic with abundant oscillatory and sector zoning. Inclusions up to 40 µm are abundant. The zircons from the *charnockites* are 100–300 µm and short to long prismatic with abundant oscillatory zoning and some are homogenous. The *lamprophyre* shows rounded 50–120 µm sub-anhedral zircons, often with dark cores and brighter rims. In all these zircons xenocrystic cores are absent.

Trace element data shows typical magmatic Th/U averages of 0.7–2.1. Their heavy over light REE enrichment is expressed by average Lu_N/Sm_N ratios of 44.3–113. All have pronounced positive Ce- and negative Eu-anomalies (Eu_N/Eu_N = 0.2–0.5).

The U-Pb concordant ages of the Várzea Alegre Pluton all give ages

Fig. 7. Representative zircon CL-images of the dated samples from the Várzea Alegre Pluton.

around 500 Ma. In detail, the gabbronorites 498 ± 7.6 Ma (VA18, Fig. 11A) and 503 ± 7.9 Ma (VA63, Fig. 11B), the two monzogranites 499 ± 7.8 Ma (VA10, Fig. 11C) and 499 ± 8.0 Ma (VA15; Fig. 11D), and the syenogranites 504 ± 8.4 Ma (VA62, Fig. 11E) and 498 ± 8.2 Ma (VA13; Fig. 11F). For the charnockites, concordia ages of 497 ± 7.8 Ma (VA42; Fig. 11G) and 502 ± 8.1 Ma (VA65; Fig. 11H) were obtained. Finally, the lamprophyre dyke (VA47) shows a somewhat younger age of 476 ± 8.9 Ma (Fig. 11I).

In the country rocks, zircons are significantly smaller, reaching 40–120 µm in size. In the *sillimanite-cordierite-biotite-garnet gneiss*, they are rounded to slightly prismatic with patchy zoning and some xenocrystic cores of 10–30 µm size. In the *garnet gneiss*, the crystals are subanhedral, mostly rounded with sector zoning, sometimes with oscillatory CL-brighter rims, some crystals, however, are homogeneous and completely luminescent.

Zircon Th/U ratios (av. 0.09–0.4) in both country rocks are lower than in the pluton, thus indicating their metamorphic origin. REE patterns are HREE enriched (Lu_N/Sm_N = 38.8–119) and show positive Ce- and negative Eu-anomalies with Eu_N/Eu_N of 0.09–0.6. The leucosome of the sill-crd-bt-grt gneiss (VA21) gives a U-Pb age of 516 ± 12 Ma (Fig. 11J), whereas the garnet-gneiss (VA49) shows much older ages, with two clusters around 899 ± 42 Ma and 617 ± 20 Ma (Fig. 11K, L). The measured zircon cores gave varying ages, likely indicating sedimented zircon populations in these metasedimentary gneisses.

4.4. Lu-Hf isotopes

All dated samples were measured for their Lu-Hf compositions (Table 1). The data for the garnet gneiss (VA49) from the Várzea Alegre Pluton is not further discussed due to its large spread and statistical uncertainty. The complete Lu-Hf data can be found in the supplementary material C.

Fig. 12A. plots εHf(t) against concordia ages showing clearly that the Venda Nova inner domain clusters around a different isotopic composition than its outer domain. The Hf-data of the inner domain all overlap within uncertainty, giving εHf(t) values between −12.3 ± 1.5 and − 8.8 ± 2.9. The different zircon core-rim U-Pb ages in the outer domain charnockites are not reflected in the Hf isotope data, which all yield εHf (t) between 3.4 ± 1.2 and 6.8 ± 1.5, *i.e.,* much closer to mantle values than any of the other lithologies. The norite has an εHf(t) of −7.3 ± 3.5, closer to the country rocks than the charnockites.

The fayalite-hedenbergite syenite yields εHf(t) values of 7.6 ± 2.6 for the 624 Ma 1st population and εHf(t) = −10.8 ± 1.5 for the 488 Ma 2nd population, fitting with the outer and inner domain, respectively. The isotopic composition of the country rock of the Venda Nova Pluton is close to that of the inner domain with εHf(t) value of −6.9 ± 6.9.

The age and εHf(t) data from the Várzea Alegre intrusion are uniform, all ages and εHf(t) overlap within uncertainty. Furthermore, the εHf(t) values of −11.1 ± 1.1 to −7.4 ± 1.3 is close to that of the Venda Nova inner domain. Várzea Alegre country rock Lu-Hf zircon data do not differ much from each other, with an εHf(t) value of −7.4 ± 3.8.

Table 1
Zircon U-Pb and Lu-Hf summary table of all measured samples from the Venda Nova and Várzea Alegre Pluton.

Sample	Lithology	Concordant/Total Analyses	Zircon concordia age ± 2σ				Event	Number of analyses (Lu-Hf)	Zircon Lu-Hf							
			Age [Ma]			MSWD			$^{176}Hf/^{177}Hf(t) \pm 2\sigma$			MSWD	εHf(t) ± 2σ			MSWD
Venda Nova inner domain																
VN65	Diorite	53/70	476.9	±	7.4	2.5	emplacement	21	0.282136	±	0.000044	0.9	−12.3	±	1.5	0.6
VN14	Quartz Syenite	60/72	490.9	±	7.5	4.9	emplacement	87	0.282226	±	0.000082	2.0	−8.8	±	2.9	1.5
VN34	Quartz Syenite	47/54	491.8	±	7.5	3	emplacement	61	0.282218	±	0.000067	2.2	−9.1	±	2.4	1.6
VN54	Quartz Syenite	38/45	480.9	±	7.5	1.6	emplacement	16	0.282151	±	0.000038	0.8	−11.7	±	1.3	0.6
VN73	Granite	62/75	491.5	±	7.6	1.8	emplacement	26	0.282173	±	0.000042	0.9	−10.7	±	1.5	0.7
VN71	Granite	63/84	486.4	±	7.5	1.5	emplacement	28	0.282184	±	0.000043	1.0	−10.4	±	1.5	0.8
Venda Nova outer domain																
VN10	Hornblende Norite	12/52	567.3	±	13.1	6.3	G2 supersuite? metamorphic overprint?	23	0.282220	±	0.000097	2.3	−7.3	±	3.4	1.3
VN56	Charnockite	31/54	619.5	±	9.7	4.1	emplacement	34	0.282575	±	0.000035	0.7	6.4	±	1.2	0.4
VN21	Charnockite	31/58	612.9	±	9.9	9.1	emplacement	24	0.282572	±	0.000053	1.2	6.2	±	1.9	0.7
VN20	Charnockite - zircon core	38/68	608.9	±	9.6	7	emplacement	32	0.282584	±	0.000060	1.1	6.5	±	2.1	0.9
	Charnockite - zircon rim	4/68	481.9	±	11.6	2.7	recrystallization	–	–	–	–	–	–	–	–	–
VN52	Charnockite - zircon core	52/104	605.7	±	9.3	1.9	emplacement	34	0.282499	±	0.000005	0.6	3.4	±	1.2	0.4
	Charnockite - zircon rim	10/104	476.2	±	7.4	5.5	recrystallization	–	–	–	–	–	–	–	–	–
VN78	Charnockite - zircon core	17/25	610.4	±	10.9	12	emplacement	15	0.282582	±	0.000018	0.2	6.5	±	0.6	0.1
	Charnockite - zircon rim	5/25	498	±	14.4	6.7	recrystallization	–	–	–	–	–	–	–	–	–
VN79	Charnockite - zircon core	30/54	613.1	±	9.8	4.9	emplacement	12	0.282592	±	0.000042	0.9	6.8	±	1.5	0.6
	Charnockite - zircon rim	5/54	499.9	±	13.9	7.9	recrystallization	–	–	–	–	–	–	–	–	–
Other																
VN32	Fayalite-Hedenbergite Syenite (1st population)	16/62	623.5	±	13.8	10	emplacement or charnockite xenocrysts?	8	0.282605	±	0.000073	0.3	7.6	±	2.6	1.4
	Fayalite-Hedenbergite Syenite (2nd population)	23/62	487.7	±	7.6	1.4	emplacement?	15	0.282172	±	0.000042	0.8	−10.8	±	1.5	0.6
VN69	Cordierite-Garnet- Sillimanite Gneiss	11/25	555.8	±	9.8	2.4	regional metamorphic peak	11	0.282239	±	0.000197	15.0	−6.92	±	7.0	11.2
Várzea Alegre																
VA18	Gabbronorite	30/34	497.7	±	7.6	0.9	emplacement	20	0.282222	±	0.000057	1.0	−8.8	±	2.0	0.8
VA10	Monzogranite	35/57	499	±	7.8	2.7	emplacement	28	0.282207	±	0.000074	1.8	−9.4	±	2.6	1.5
VA63	Gabbronorite	31/39	502.5	±	7.9	3.2	emplacement	18	0.282220	±	0.000047	0.7	−8.8	±	1.7	0.5
VA62	Syenogranite	31/50	503.5	±	8.4	5.7	emplacement	20	0.282193	±	0.000066	1.3	−9.7	±	2.4	1.1
VA13	Syenogranite	15/34	498.3	±	8.2	2.5	emplacement	8	0.282204	±	0.000059	1.3	−9.5	±	2.1	1.1
VA15	Monzogranite	53/68	498.7	±	8.0	5.5	emplacement	30	0.282156	±	0.000030	0.3	−11.1	±	1.1	0.2
VA42	Charnockite	47/49	497.3	±	7.8	4	emplacement	29	0.282228	±	0.000049	0.8	−8.6	±	1.8	0.7
VA65	Charnockite	31/48	501.5	±	8.1	4.8	emplacement	27	0.282259	±	0.000037	0.5	−7.4	±	1.3	0.4
VA47	Lamprophyre	16/31	475.6	±	8.9	12	emplacement	16	0.282260	±	0.000065	1.0	−8.0	±	2.3	0.7
VA21	Sillimanite-Cordierte-Biotite-Garnet Gneiss	14/22	516.1	±	12.0	19	regional metamorphic peak	15	0.282251	±	0.000107	1.4	−7.4	±	3.8	1.2
VA49*	Garnet Gneiss	7/30	899.4	±	42.2	23	rifting stage?	21	0.282111	±	0.000679	156	−3.7	±	24	77
		5/30	616.9	±	19.9	23	recrystallization?	21	0.282119	±	0.000682	157	−9.8	±	24	94

* Lu-Hf data for sample VA49 not further discussed due to high statistical uncertainty (see supplementary material C).

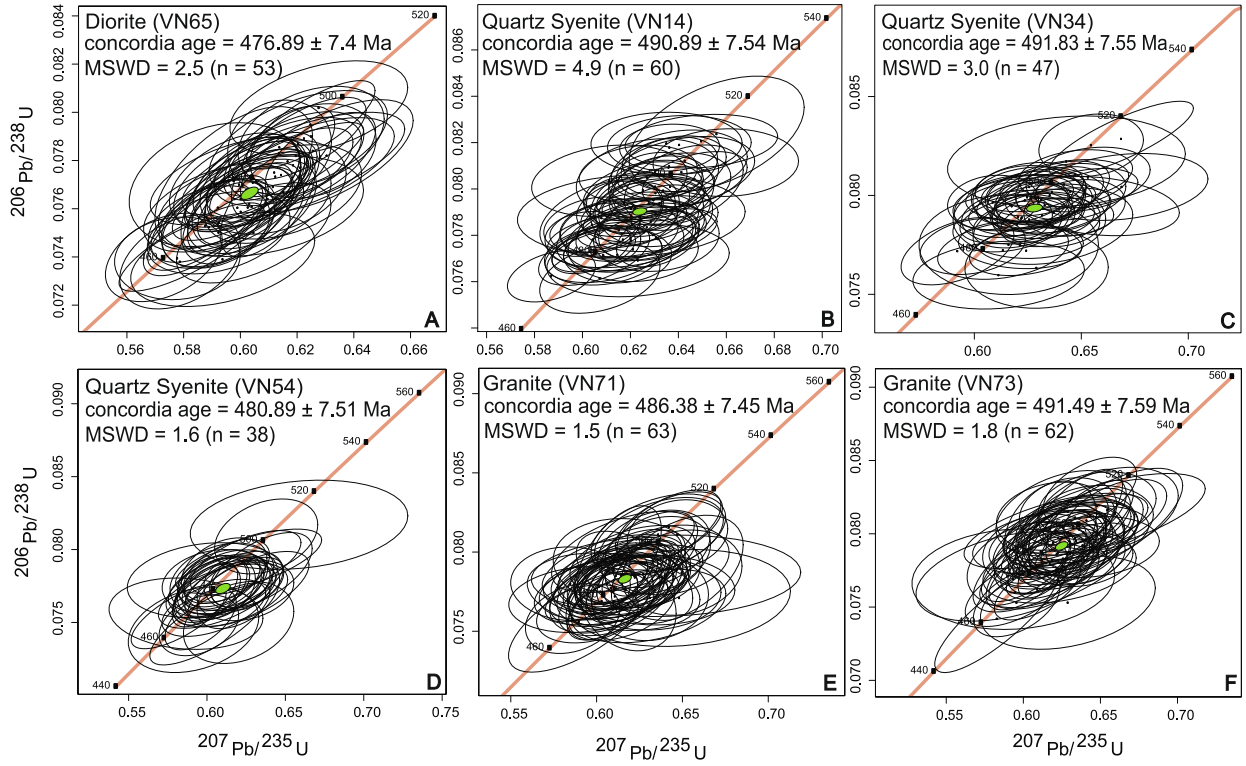

Fig. 8. Wetherill diagram for the samples from the Venda Nova inner domain. Error ellipses are 2σ.

5. Discussion

5.1. Timing of magmatism

The six dated samples from the inner domain of the Venda Nova Pluton yield concordia ages of 492–477 Ma, individual ages, based on 38–63 concordant analyses have 2σ errors of typically 7–8 Ma. These ages represent the intrusion age(s) of the Venda Nova inner domain, no textural domains in zircons or statistically distinct age groups can be identified. Statistically, these ages are indistinct, nominally they yield a period of 15 Ma. Our ages fit well with the recent ages of an inner domain quartz syenite of 497 ± 4 Ma and gabbronorite of 501 ± 4 Ma (Bellon et al., 2022). Further, this range fits well with other ages of the G5 suite, *i.e.,* the post-collisional magmatism that occurred in this region 520–480 Ma ago (*e.g.* De Campos et al., 2016; Pedrosa-Soares et al., 2001, 2011).

In contrast, the outer charnockite ring of the Venda Nova Pluton has a crystallization age of 620–606 ± 11 Ma, belonging age-wise to the calc-alkaline arc magmatism, *i.e.,* to the pre-collisional subduction-related magmatism predating this orogen (G1 suite). Our data show that some outer domain zircon rims recrystallized during intrusion of the inner domain, 4 of 6 charnockite zircon samples yield rim ages of 500–476 ± 14 Ma. Note that these rims are indistinct in εHf(t), indicating a mechanism of ring formation that excludes Lu-Hf disturbance. This argues either for a thermal disturbance or partial melting due to fluid-infiltration (Hf and Lu being completely insoluble in such fluids) during the emplacement of the ~500 Ma inner domain. The most likely scenario is minor fluid-saturated remelting of the charnockites triggered by the fluids expulsed from the crystallizing magmas of the inner domain, yet, fluid-mediated recrystallization without remelting cannot be excluded. This interpretation is consistent with Bellon et al. (2022), who attribute their charnockite sample to the G1 suite, yet observe a second zircon rim age interpreted as thermal resetting during emplacement of the inner domain.

The fayalite-hedenbergite syenite has two age-wise and morphologically distinct zircon populations, the older age group corresponding to smaller rounded zircons, the younger age group to large oscillatory zoned zircons. Importantly, the 623 ± 14 Ma old zircons have the same positive εHf isotopic range as the charnockites from the Venda Nova outer domain, in contrast, the oscillatory zoned 488 ± 8 Ma zircons the same negative εHf range as the inner domain lithologies. These fayalite-hedenbergite syenites are small isolated bodies within the inner domain, the poor outcrop quality impeding the observation of contact relations. It is likely that they were emplaced at around 620 Ma, but, as enclosed in the inner domain, have been more heated than the outer charnockite rim, and plausibly infiltrated by Lu + Hf transporting melts of the inner domain, leading to a new zircon population with inner domain εHf(t) values. The older zircon group is age-wise similar to the zircon cores of the charnockites and shows similar zircon REE-patterns. Another possibility would be that the emplacement of the fayalite-hedenbergite syenite is simultaneous to the inner domain at around 500 Ma, and that the older zircon population are recrystallized charnockitic xenocrysts. An inheritance for these older zircons from *e.g.* country rock metapelites seems unlikely as these would not show mantle-like isotopic signatures (positive εHf(t)). Nevertheless, in bulk rock chemistry and mineralogy, these ferro-syenites do neither fit with the inner nor outer domain (Fig. 5A). We cannot exclude that this lithology might represent an independent magmatic lineage with respect to the outer and inner domains. In any case, these syenites are more evolved than any other Venda Nova lithology, further study is needed to better constrain their genesis.

Interestingly, the norite from the outer domain rim and the cordierite-garnet-sillimanite gneiss show similar εHf and similar ages of ~560 Ma, which represents the orogenic metamorphic thermal peak leading to granulite facies and a voluminous S-type granite magmatism in the region (the G2 suite, *e.g.* Pedrosa-Soares et al., 2008). Likely, the norite was metamorphically overprinted, in fact, the 12 concordant data points show a wide spread of ages, ranging from 610 to 550 Ma, leaving some leeway for interpretation. One could argue that the norites are the heat source responsible for this regions anatexis of the G2-granitoids.

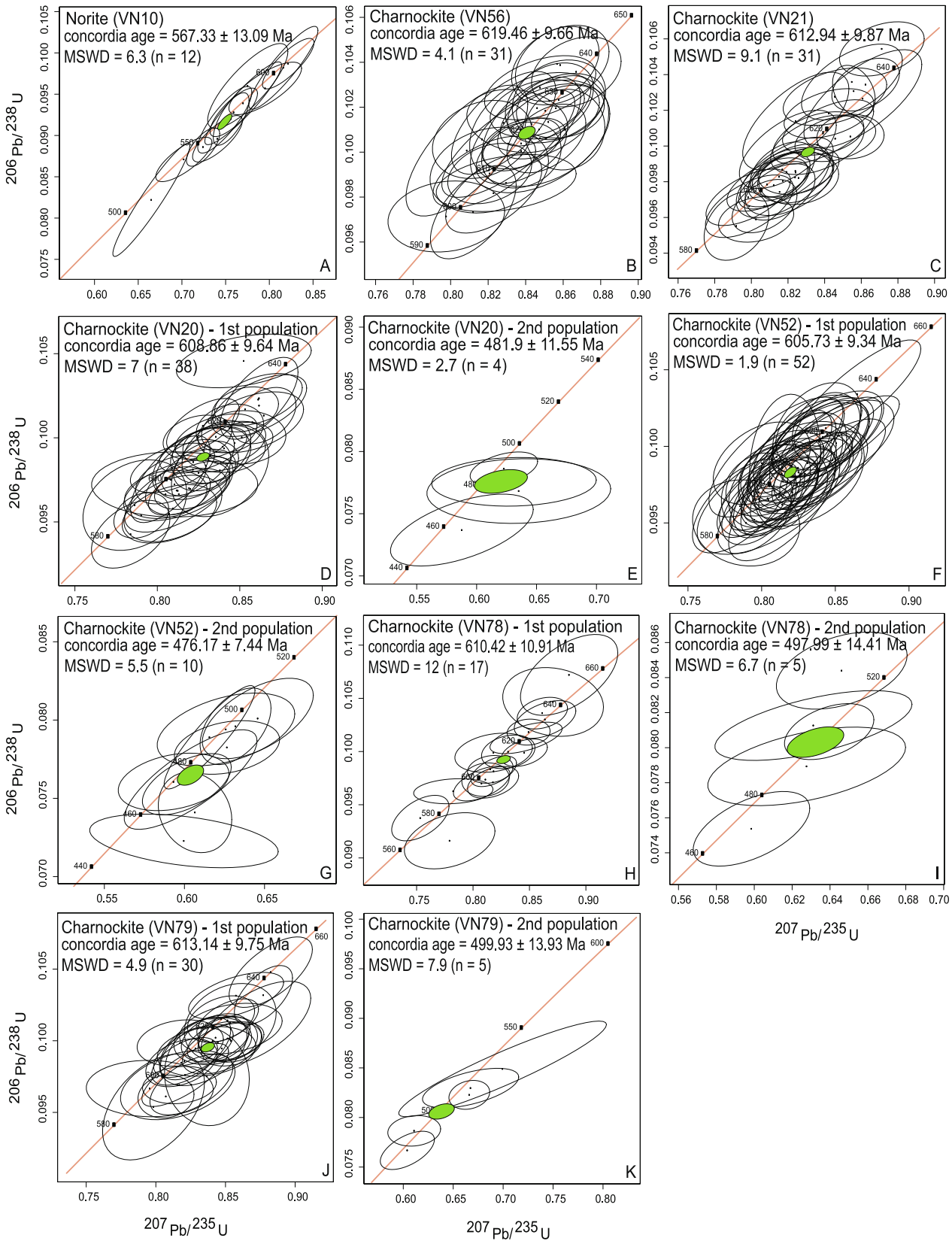

Fig. 9. Wetherill diagram for the samples from the Venda Nova outer domain. Error ellipses are 2σ.

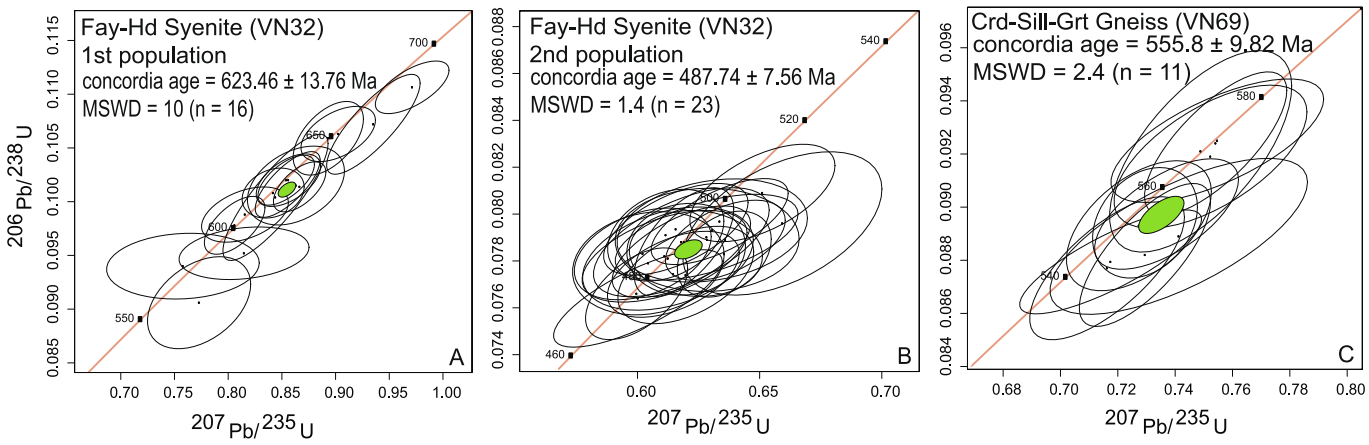

Fig. 10. Wetherill diagram for the fayalite-hedenbergite syenite and country rock from Venda Nova.

However, this seems unlikely since these norites and other mafic lithologies of similar age are volumetrically irrelevant through the Araçuaí belt.

For the Várzea Alegre Pluton, the U-Pb data yield one magmatic age at around 500 ± 8 Ma with the lamprophyre dike intruding about 20 Ma later. Apparently, the gabbronorites, monzogranites, syenogranites and charnockites, all belong to one magmatic pulse. This confirms the interpretation of Mendes et al. (2005) who, dating one charnockite, refuted the notion that the charnockitic unit is an earlier magmatic pulse (as proposed by Medeiros et al., 2000).

Lithologically, there is little difference between the ~612 Ma old charnockites from the Venda Nova Pluton and the ~500 Ma charnockites from the Várzea Alegre Pluton. Nevertheless, the former belongs geotectonically to the calc-alkaline subduction-related G1 suite, the latter to the mildly alkaline post-orogenic G5 suite. Geochemically, the charnockites from Venda Nova are calc-alkaline, calcic, metaluminous, more magnesian and depleted in incompatible elements. In contrast, the Várzea Alegre charnockites are mildly alkaline, more ferroan and enriched in K and incompatible elements, fitting well with the post-orogenic G5 magmatism of the Araçuaí belt.

5.2. Source of magmatism

The ~612 Ma old charnockites from the Venda Nova outer domain show zircon εHf values that are moderately positive, indicating a juvenile depleted mantle source. Such values are exceptional in the regional context, as positive εHf or εNd is nowhere reported in the literature on the Araçuaí belt (Fig. 12A,C). Two charnockite samples from the Venda Nova Pluton were measured for Sr and Nd-isotopes (De Campos et al., 2016), but were assumed to be 500 Ma old. *Re*-correcting these data for 600 Ma, the isotopic values still give negative εNd (−5 and − 2.3) and high $^{87}Sr/^{86}Sr$ ratios (0.7058 and 0.7072), indicating a crustally enriched source. Other G1 lithologies from the magmatic arc (mostly located further west in the Araçuaí belt), have generally more radiogenic Hf and Nd magmatic signatures than observed for the Venda Nova outer domain (in εHf). Only Tupinambá et al. (2012) reported bulk εNd values of +0.2 to +1.8 from the Rio Negro Complex in the Ribeira belt, ~300 km to the South, with a similar age (630 Ma) as the charnockites from the Venda Nova Pluton. The Venda Nova G1 suite may thus be rather an exception for the calc-alkaline 630–580 Ma G1 magmatism in the region. Possible explanations for different εNd and εHf signatures could be chemically and isotopically heterogenous mantle domains with varying contributions of subducted oceanic crust, or asthenospheric upwelling from a deeper mantle section.

The Hf-data for the inner domain of the Venda Nova and the entire Várzea Alegre Plutons show all negative εHf values across a narrow range (Fig. 12A,B), albeit slightly less negative for the Várzea Alegre Pluton. These Hf-values are consistent with published Sm-Nd isotopic data for both plutons, which have been interpreted as reflecting a mixture of interacting mantle and crustal melts (De Campos et al., 2016; Medeiros et al., 2003; Wiedemann et al., 2002) but may equally reflect a (lithospheric) mantle source contaminated by crustal material (source assimilation). Macêdo et al. (2022) reports Hf isotopic values in zircon for three samples of the Castelo Pluton. Their measured monzogranite give εHf values of 2.5 ± 15, plotting into the depleted mantle field, but the large isotopic scatter makes these results inconclusive for our study.

In principle, the observed gabbroic parent magmas of these plutons can only derive from the mantle and not by the melting of continental crust. Primitive magmas with low $^{176}Hf/^{177}Hf$ and negative εHf (as well as low $^{143}Nd/^{144}Nd$ and high $^{87}Sr/^{86}Sr$) likely arise from contaminated lithospheric mantle, into which the signature of ancient continental material has been introduced. The least evolved gabbro(noritic) intrusives of both plutons are not primitive, but already have a lesser X_{Mg}, thus, at present, it remains open whether the crustal εHf of these intrusives stems from and is already present in the mantle, *i.e.,* a (likely subduction) modified and metasomatized lithosphere, or whether this crustal signature is acquired during early assimilation in the crust. Notably, the εHf values remain constant across the entire differentiation series, thus if path contamination led to these isotopic signatures, this happened at the early stage when magmatic temperatures were higher. Remarkably, the country rocks measured show less negative εHf than the magmatic samples, rendering them unsuitable as (the only) contaminants. The same applies to the crustal G2 suite. Here too εHf is less negative than the magmatic rocks (see Fig. 12A), making them unlikely to have acted as contaminants. This strongly argues in favor of mantle source contamination, possibly through the metasomatic agent released from the subducting Adamastor-ocean slab at ~650–600 Ma (Gradim et al., 2014; Pedrosa-Soares et al., 2011), or possibly of more ancient origin, *i.e.,* in the subcontinental lithosphere of the Congo craton. It is important to stress that such a metasomatic process does not lead to a homogenously contaminated mantle (*e.g.* Pilet et al., 2008). Such heterogeneities may then reflect in the chemistry and isotopic signatures of the various post-collisional plutons. The Venda Nova inner domain and Várzea Alegre Pluton both show isotopically enriched signatures with the samples from Várzea Alegre being slightly less negative in εHf.

The magmatic source for the charnockites from the Venda Nova outer domain was a depleted and K-poor mantle, in contrast to both the inner domain and the Várzea Alegre pluton. Moreover, path contamination, *i.e.*, assimilation in the crust, was very minor. The isotopic differences of the charnockites of this study and those from other post-collisional G5 plutons measured by De Campos et al. (2016) could be interpreted either as melting of differently metasomatized mantle

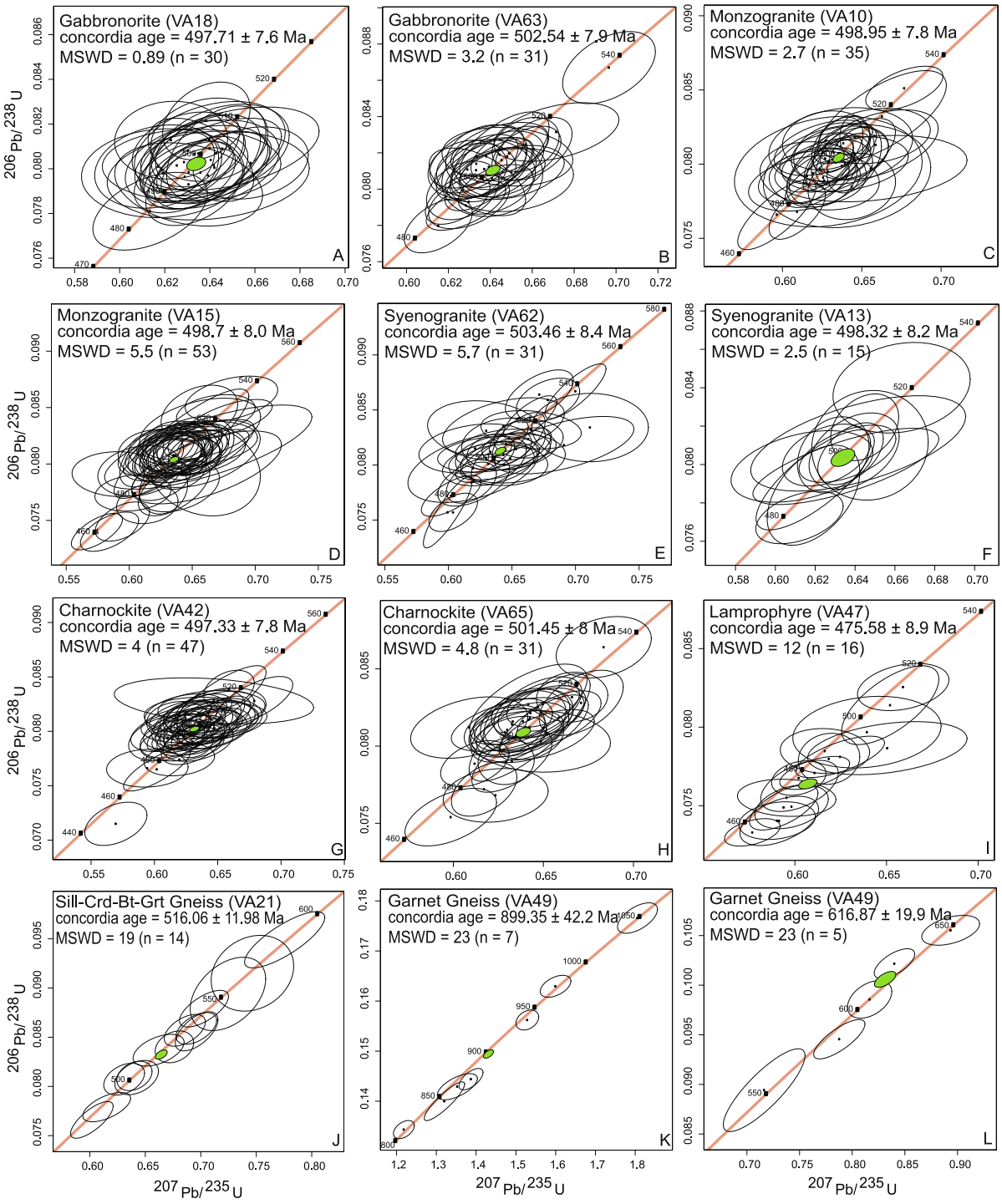

Fig. 11. Wetherill diagram for the samples from the Várzea Alegre Pluton. Error ellipses are 2σ.

domains or as different degrees of contamination during ascent and emplacement in the crust.

5.3. Implications for understanding post-collisional magmatism in the Araçuaí belt

The Venda Nova and Várzea Alegre Plutons formed at the final stage of a Wilson cycle, contributing a small but not negligible ultimate fraction to crustal growth when compared to arc magmatism. During the relaxation phase of the Brasiliano orogeny, the post-orogenic magmatic activity (G5) led to various plutons which range from calc-alkaline to mildly alkaline compositions, likely reflecting a significant mantle heterogeneity. The most likely scenario is that the melts for both post-collisional plutons derive from the subcontinental lithospheric mantle affected in variables degrees by metasomatic agent(s). This contamination may stem from the previous subduction magmatism generating high-K and LILE now observed in the measured rocks, yet a more ancient metasomatism, which had possibly occurred below the Congo craton before subduction of the Adamastor ocean, cannot be excluded. Regardless of its origin, a stronger (high-K) contamination appears to lead to more alkaline magma types (Venda Nova inner domain with dominant syenites), while a lesser contamination to alkaline/calc-

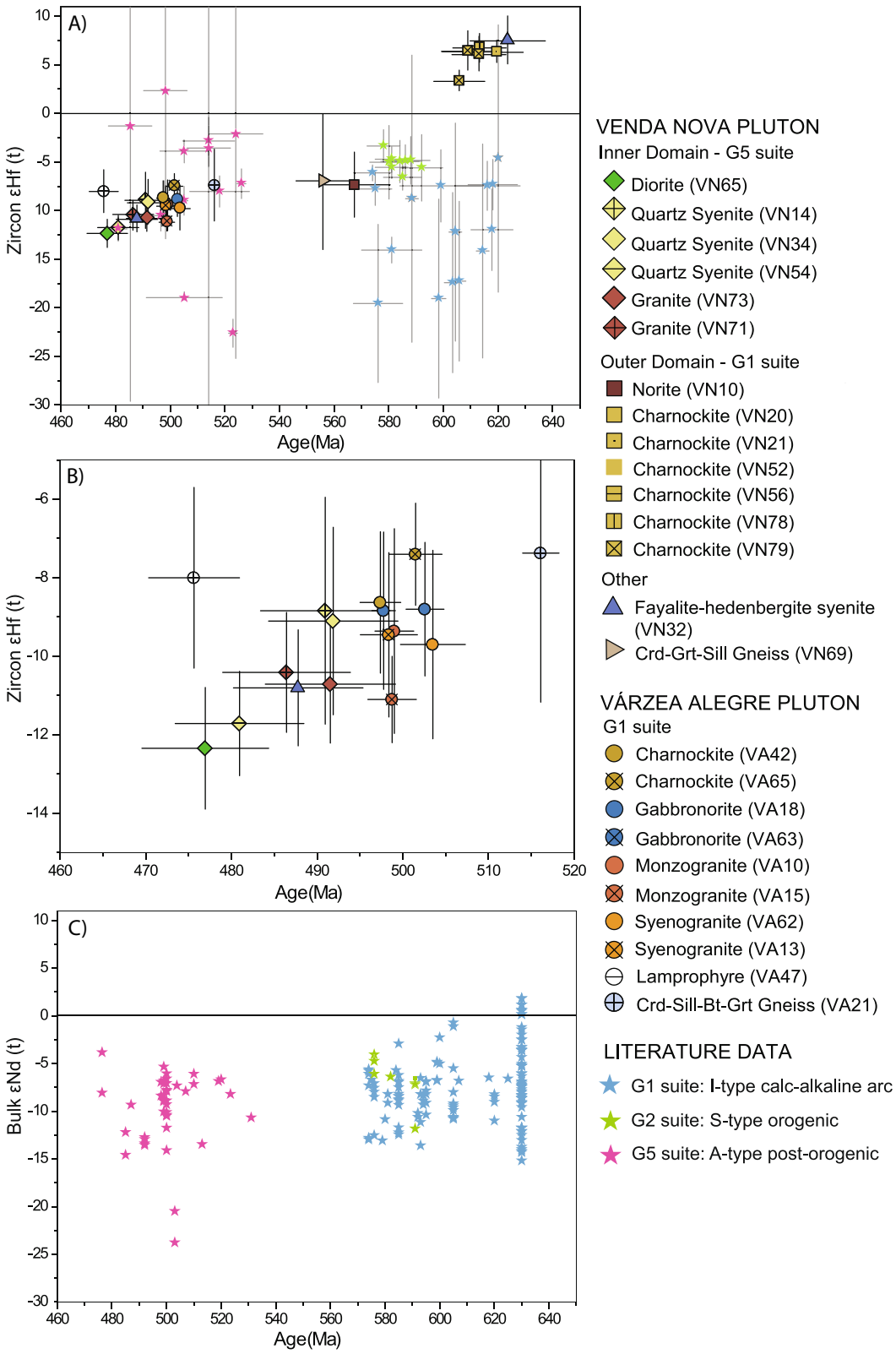

Fig. 12. A) Concordia ages (Ma) *versus* average εHf(t) of the Venda Nova inner domain, outer domain and Várzea Alegre Pluton. Colours of the data point represent the lithology as in the geological map. Error bars are 2σ. Literature data of hafnium isotopic data for the G1 suite from Gonçalves et al. (2016), Tedeschi et al. (2016), Araujo et al. (2020), Santiago et al. (2022) and Schannor et al. (2020); for the G2 suite from Melo et al. (2017), and Araujo et al. (2020); and for the G5 suite from Aranda et al. (2020), Araujo et al. (2020), Melo et al. (2020), Santiago et al. (2020) and Macêdo et al. (2022). B) Enlarged view of the data points from the Venda Nova and Várzea Alegre Pluton. C) Concordia ages (Ma) *versus* the average bulk εNd(t) of data taken from the literature. G1 suite from Nalini Júnior et al. (2000), Martins et al. (2004), Gonçalves (2009), Mendes et al. (2010), Pedrosa-Soares et al. (2011), Tupinambá et al. (2012), Heilbron et al. (2013), Gonçalves et al. (2016), Tedeschi et al. (2016), De Campos et al. (2004, 2016), Peixoto et al. (2017) and Soares et al. (2020); G2 suite from Martins et al. (2004); and G5 suite from Mello (2000), Wiedemann et al. (2002), Medeiros et al. (2003), Martins et al. (2004), Fleck (2014) and De Campos et al. (2016).

alkaline types (Várzea Alegre with dominant charnockites, monzo- and syeno-granites) yet still not akin to classical calc-alkaline batholiths (with a diorite-tonalite-granodiorite-granite suite).

Further, the role of path contamination, *i.e.,* assimilation within the continental crust *versus* source contamination for a magmatic series may be challenging to identify in this kind of setting. Even though post-collisional magma series begin with mantle-derived melts, they are susceptible to path contamination as they pass through the over-thickened crust to reach intermediate crustal levels. So far, the Lu-Hf isotopic system on zircons indicates minor assimilation during the observable range of magma evolution, crystal fractionation was, hence, the primary process for rock differentiation during the observable part of the G5 post-orogenic magmatism.

6. Conclusions

Our extensive geochronological data link the emplacement of the Venda Nova inner domain to the 500 Ma post-collisional magmatism of the Araçuaí belt. The Venda Nova outer domain, dominated by a charnockitic rim, is not coeval, crystallization ages of around 620–606 Ma align with the pre-collisional magmatism in this area. Nevertheless, the combination of zircon morphology, Lu-Hf isotopic data and rim ages yields a clear overprint at 500 Ma that requires a process closed for Hf-isotopes. Likely, this involved an infiltration of deuteric fluids from the inner domain into the outer domain, causing partial fluid-saturated re-melting therein. This behavior contrasts with the fayalite-hedenbergite syenite found within the inner domain. This rock type could have intruded contemporaneously with the charnockitic body, in which case the zircons underwent significant reheating and recrystallization during the intrusion of the inner domain. Alternatively, the fayalite-hedenbergite syenite intruded with the inner domain lithologies, in which case, the older zircons (with positive εHf) could correspond to xenocrysts from the charnockite.

In contrast to Venda Nova, the Várzea Alegre Pluton is (i) the product of one magmatic period at ~500 Ma and (ii) has a thick charnockite rim that is co-magmatic and co-genetic with the inner part. At the outcrop level, the Várzea Alegre charnockite amounts to about half of the entire intrusive volume, indicating that contact-related processes did not play a major role in their genesis.

In terms of source, we interpret the Venda Nova inner domain and the Várzea Alegre Pluton as products of melts derived from a lithospheric mantle that has been previously enriched by crustal material. Nevertheless, truly primitive magmas are not available, thus an early contamination in the crust of such magmas that could have led to the least differentiated accessible magmas, the gabbro(norite)s cannot be excluded. In contrast, the Venda Nova outer domain charnockites derived from a mantle that has not been chemically altered and the differentiation from primitive melts to charnockites and their emplacement was not accompanied by assimilation with crustal material. As a consequence, the charnockites from the Venda Nova outer domain and the Várzea Alegre Pluton formed not only 100 Ma apart, but show very contrasting geochemical and isotopic compositions. To conclude, path contamination likely played a minor role in each pluton, documented in relatively homogenous Hf-isotopic values and the lack of older xenocrystic zircons.

Supplementary data to this article can be found online at https://doi.org/10.1016/j.lithos.2024.107677.

CRediT authorship contribution statement

Clara Talca Onken: Writing – original draft, Visualization, Investigation, Formal analysis, Conceptualization. **Jessica Eberhard-Schmid:** Investigation. **Livia Hauser:** Investigation. **Simone Marioni:** Investigation. **Andrea Galli:** Writing – review & editing, Supervision, Conceptualization. **Valdecir de Assis Janasi:** Writing - review & editing, Conceptualization. **Max W. Schmidt:** Writing – review & editing, Supervision, Funding acquisition, Conceptualization.

Declaration of competing interest

The authors declare that they have no known competing financial interests or personal relationships that could have appeared to influence the work reported in this paper.

Acknowledgments

This project was funded by the Grubenmann-Burri Fond, ETH Zurich. Andreas Jallas, Lydia Zehnder and Marcel Guillong are thanked for help with the laboratory facilities. Constructive comments from Bernard Bonin and an anonymous reviewer, along with the editorial handling of Greg Shellnutt, are gratefully acknowledged.

References

Alkmim, F.F., Marshak, S., Pedrosa-Soares, A.C., Peres, G.G., Cruz, S.C.P., Whittington, A., 2006. Kinematic evolution of the Araçuaí-West Congo orogen in Brazil and Africa: nutcracker tectonics during the Neoproterozoic assembly of Gondwana. Precambrian Res. 149 (1–2), 43–64.

Amaral, L., de Andrade Caxito, F., Pedrosa-Soares, A.C., Queiroga, G., Babinski, M., Trindade, R., Chemale, F., 2020. The Ribeirão da Folha ophiolite-bearing accretionary wedge (Araçuaí orogen, SE Brazil): new data for Cryogenian plagiogranite and metasedimentary rocks. Precambrian Res. 336, 105522.

Anderson, D.L., 2005. Large igneous provinces, delamination, and fertile mantle. Elements 1 (5), 271–275.

Aranda, R.D.O., Chaves, A.D.O., Júnior, E.M., Junior, R.V., 2020. Petrology of the Afonso Cláudio intrusive complex: new insights for the cambro-ordovician post-collisional magmatism in the Araçuaí-West Congo orogen, Southeast Brazil. J. S. Am. Earth Sci. 98, 102465.

Araujo, C., Pedrosa-Soares, A., Lana, C., Dussin, I., Queiroga, G., Serrano, P., Medeiros-Júnior, E., 2020. Zircon in emplacement borders of post-collisional plutons compared to country rocks: a study on morphology, internal texture, U–Th–Pb geochronology and Hf isotopes (Araçuaí orogen, SE Brazil). Lithos 352, 105252.

Balashov, Y.A., Glaznev, V.N., 2006. Cycles of alkaline magmatism. Geochem. Int. 44 (3), 274–285.

Bellon, U.D., Junior, G.S., Temporim, F.A., D'Agrella-Filho, M.S., Trindade, R.I.F., 2022. U-Pb geochronology of a reversely zoned pluton: records of pre-to-post collisional magmatism of the Araçuaí belt (SE-Brazil)? J. S. Am. Earth Sci. 119, 104045.

Belousova, E.A., Griffin, W.L., O'Reilly, S.Y., 2006. Zircon crystal morphology, trace element signatures and Hf isotope composition as a tool for petrogenetic modelling: examples from Eastern Australian granitoids. J. Petrol. 47 (2), 329–353.

Bouvier, A., Vervoort, J.D., Patchett, P.J., 2008. The Lu-Hf and Sm-Nd isotopic composition of CHUR: constraints from unequilibrated chondrites and implications for the bulk composition of terrestrial planets. Earth Planet. Sci. Lett. 273 (1–2), 48–57.

Cavalcante, C., Fossen, H., de Almeida, R.P., Hollanda, M.H.B., Egydio-Silva, M., 2019. Reviewing the puzzling intracontinental termination of the Araçuaí-West Congo orogenic belt and its implications for orogenic development. Precambrian Res. 322, 85–98.

Cornet, J., Laurent, O., Wotzlaw, J.F., Antonelli, M.A., Otamendi, J., Bergantz, G.W., Bachmann, O., 2022. Reworking subducted sediments in arc magmas and the isotopic diversity of the continental crust: the case of the Ordovician Famatinian crustal section, Argentina. Earth Planet. Sci. Lett. 595, 117706.

De Campos, C.P., Mendes, J.C., Ludka, I.P., Medeiros, S.R., Moura, J.C., Wallfass, C., 2004. A review of the Brasiliano magmatism in southern Espírito Santo, Brazil, with emphasis on postcollisional magmatism. J. Virtual Explor. 17 (1), 35.

De Campos, C.P., de Medeiros, S.R., Mendes, J.C., Pedrosa-Soares, A.C., Dussin, I., Ludka, I.P., Dantas, E.L., 2016. Cambro-Ordovician magmatism in the Araçuaí Belt (SE Brazil): snapshots from a post-collisional event. J. S. Am. Earth Sci. 68, 248–268.

Fleck, J.B.F., 2014. Geoquímica, geocronologia e contexto geotectônico do magmatismo máfico associado ao Feixe de Fraturas Colatina, Estado Espirito Santo.

Fossen, H., Cavalcante, G.C., de Almeida, R.P., 2017. Hot versus cold orogenic behavior: comparing the Araçuaí-West Congo and the Caledonian orogens. Tectonics 36 (10), 2159–2178.

Frost, B.R., Frost, C.D., 2008. On charnockites. Gondwana Res. 13 (1), 30–44.

Frost, B.R., Frost, C.D., Hulsebosch, T.P., Swapp, S.M., 2000. Origin of the charnockites of the Louis lake Batholith, wind River Range, Wyoming. J. Petrol. 41 (12), 1759–1776.

Gonçalves, L.E.D.S., 2009. Características gerais e história deformacional da suíte granítica G1, entre Governador Valadares e Ipanema, MG.

Gonçalves, L., Alkmim, F.F., Pedrosa-Soares, A.C., Dussin, I.A., Valeriano, C.D.M., Lana, C., Tedeschi, M., 2016. Granites of the intracontinental termination of a magmatic arc: an example from the Ediacaran Araçuaí orogen, southeastern Brazil. Gondwana Res. 36, 439–458.

Gradim, C., Roncato, J., Pedrosa-Soares, A.C., Cordani, U., Dussin, I., Alkmim, F.F., Babinski, M., 2014. The hot back-arc zone of the Araçuaí orogen, Eastern Brazil: from sedimentation to granite generation. Braz. J. Geol. 44 (1), 155–180.

Guillong, M., Meier, D.L., Allan, M.M., Heinrich, C.A., Yardley, B.W., 2008. Appendix A6: SILLS: a MATLAB-based program for the reduction of laser ablation ICP-MS data of homogeneous materials and inclusions. Mineral. Assoc. Canada Short Cour. 40, 328–333.
Heilbron, M., Machado, N., 2003. Timing of terrain accretion in the Neoproterozoic-Eoproterozoic Ribeira orogen, (SE Brazil). Precambrian Res. 125, 97–112.
Heilbron, M., Tupinambá, M., de Morisson Valeriano, C., Armstrong, R., do Eirado Siva, L.G., Melo, R.S., Machado, N., 2013. The Serra da Bolívia complex: the record of a new Neoproterozoic arc-related unit at Ribeira belt. Precambrian Res. 238, 158–175.
Horn, H.A., Weber-Diefenbach, K., 1987. Geochemical and genetic studies of three invers zoned intrusive bodies of both alkaline and calc-alkaline composition in the Ribeira mobile belt, Espirito Santo, Brazil. Rev. Brasil. Geoci. 17 (4), 488–497.
Hoskin, P.W., Ireland, T.R., 2000. Rare earth element chemistry of zircon and its use as a provenance indicator. Geology 28 (7), 627–630.
Janasi, V.A., 2002. Elemental and Sr-Nd isotope geochemistry of two Neoproterozoic mangerite suites in SE Brazil: implications for the origin of the mangerite-charnockite-granite series. Precambrian Res. 119 (1–4), 301–327.
Kilpatrick, J.A., Ellis, D.J., 1992. C-type magmas: igneous charnockites and their extrusive equivalents. Earth Environ. Sci. Trans. R. Soc. Edinb. 83 (1–2), 155–164.
Landoll, J.D., 1994. The role of crustal interactions in the formation of cogenetic silica oversaturated and undersaturated syenites: Evidence from the alkaline complexes of Abu Khruq (Egypt). In: Mt. Shefford (Quebec), and Marangudzi (Zimbabwe). The Ohio State University.
Liegeois, J.P., Navez, J., Hertogen, J., Black, R., 1998. Contrasting origin of post-collisional high-K calc-alkaline and shoshonitic versus alkaline and peralkaline granitoids. The use of sliding normalization. Lithos 45 (1–4), 1–28.
Ludka, I.P., Wiedemann, C.M., Töpfner, C., 1998. On the origin of incompatible element enrichment in the Venda Nova pluton, State of Espírito Santo, Southeast Brazil. J. S. Am. Earth Sci. 11 (5), 473–486.
Macêdo, I.M.L., Geraldes, M.C., de Abreu Marques, R., de Melo, M.G., Tavares, A.D., Martins, M.V.A., Rodrigues, R.D., 2022. New clues for magma-mixing processes using petrological and geochronological evidence from the Castelo Intrusive complex, Araçuaí Orogen (SE Brazil). J. S. Am. Earth Sci. 115, 103758.
Martins, V.T.D.S., Teixeira, W., Noce, C.M., Pedrosa-Soares, A.C., 2004. Sr and Nd characteristics of Brasiliano/Pan-African granitoid plutons of the Araçuaí Orogen, Southeastern Brazil: tectonic implications. Gondwana Res. 7 (1), 75–89.
McKenzie, D., O'Nions, R.K., 1983. Mantle reservoirs and ocean island basalts. Nature 301 (5897), 229–231.
Medeiros, S.R., Wiedemann, C.M., Mendes, J.C., 2000. Post-collisional magmatism in the Araçuaí-Ribeira Mobile belt: geochemical and isotopic study of the Várzea Alegre intrusive complex (VAIC), ES, Brazil. Rev. Bras. Geoci. 30 (1), 30–34.
Medeiros, S.R., Wiedemann-Leonardos, C.M., Vriend, S., 2001. Evidence of mingling between contrasting magmas in a deep plutonic environment: the example of Várzea Alegre, in the Ribeira Mobile Belt, Espírito Santo, Brazil. An. Acad. Bras. Cienc. 73, 99–119.
Medeiros, S.R., Mendes, J.C., McReath, I., Wiedemann, C.M., 2003. U-Pb and Rb-Sr Dating and Isotopic Signature of the Charnockitic Rocks from Várzea Alegre Intrusive Complex, Espírito Santo, Brazil. Short Papers.
Mello, F.M.D., 2000. Litogeoquímica e química mineral do Maciço Charnockítico Aimorés-MG (Doctoral dissertation,. Universidade de São Paulo.
Melo, M.G., Lana, C., Stevens, G., Pedrosa-Soares, A.C., Gerdes, A., Alkmin, L.A., Alkmim, F.F., 2017. Assessing the isotopic evolution of S-type granites of the Carlos Chagas Batholith, SE Brazil: clues from U–Pb, Hf isotopes, Ti geothermometry and trace element composition of zircon. Lithos 284, 730–750.
Melo, M.G., Lana, C., Stevens, G., Hartwig, M.E., Pimenta, M.S., Nalini Jr., H.A., 2020. Deciphering the source of multiple U–Pb ages and complex Hf isotope composition in zircon from post-collisional charnockite-granite associations from the Araçuaí orogen (southeastern Brazil). J. S. Am. Earth Sci. 103, 102792.
Mendes, J.C., De Campos, C.M., 2012. Norite and charnockites from the Venda Nova Pluton, SE Brazil: intensive parameters and some petrogenetic constraints. Geosci. Front. 3 (6), 789–800.
Mendes, J.C., Wiedemann, C.M., McReath, I., 2002. Norito e charnoenderbitos da borda do maciço intrusivo de Venda Nova, Espírito Santo. Anu. Inst. Geocienc. 25, 99–124.
Mendes, J.C., de Medeiros, S.R., McReath, I., de Campos, C.M.P., 2005. Cambro-Ordovician magmatism in SE Brazil: U-Pb and Rb-Sr ages, combined with Sr and Nd isotopic data of charnockitic rocks from the Varzea Alegre complex. Gondwana Res. 8 (3), 337–345.
Mendes, J.C., McReath, I.A.N., Wiedemann, C.M., Figueiredo, M C.H.D., 1997. Charnockitóides do Maciço de Várzea Alegre: um novo exemplo do Magmatismo cálcio-alcalino de alto-K no arco magmático do Espírito Santo. Revista Brasileira de Geociências 27 (1), 13–24.
Mendes, J.C., Medeiros, S.R., Ludka, I.P., Pereira, T., Silva, P.D., 2010. Age and Nd-Sr results of an arc-related hornblende orthogneiss from the border of the Ribeira and Araçuaí belts. In: Anais, VII SSAGI, South American Symposium on Isotope Geology, Brasília, Electronic Edition.
Middlemost, E.A., 1994. Naming materials in the magma/igneous rock system. Earth Sci. Rev. 37 (3–4), 215–224.
Mücke, A., 2003. Fayalite, pyroxene, amphibole, annite and their decay products in mafic clots within Younger Granites of Nigeria: petrography, mineral chemistry and genetic implications. J. Afr. Earth Sci. 36 (1–2), 55–71.
Nalini Júnior, H.A., Bilal, E., Neves, J.M.C., 2000. Syn-collisional peraluminous magmatism in the Rio Doce region: mineralogy, geochemistry and isotopic data of the Urucum suite (eastern Minas Gerais state, Brazil).
Neves, B.B.B., Cordani, U.G., 1991. Tectonic evolution of South America during the late Proterozoic. Precambrian Res. 53 (1–2), 23–40.
Newton, R.C., Smith, J.V., Windley, B.F., 1980. Carbonic metamorphism, granulites and crustal growth. Nature 288, 45–50.
Paton, C., Hellstrom, J., Paul, B., Woodhead, J., Hergt, J., 2011. Iolite: freeware for the visualisation and processing of mass spectrometric data. J. Anal. At. Spectrom. 26 (12), 2508–2518.
Pedrosa-Soares, A.C., Noce, C.M., Wiedemann, C.M., Pinto, C.P., 2001. The Araçuaı-West-Congo Orogen in Brazil: an overview of a confined orogen formed during Gondwanaland assembly. Precambrian Res. 110 (1–4), 307–323.
Pedrosa-Soares, A.C., Alkmim, F.F., Tack, L., Noce, C.M., Babinski, M., Silva, L.C.D., Martins-Neto, M.A., 2008. Similarities and differences between the Brazilian and African counterparts of the Neoproterozoic Araçuaí-West Congo orogen. Geol. Soc. Lond. Spec. Publ. 294 (1), 153–172.
Pedrosa-Soares, A.C., De Campos, C.P., Noce, C., Silva, L.C., Novo, T., Roncato, J., Alkmim, F., 2011. Late Neoproterozoic-Cambrian granitic magmatism in the Araçuaí orogen (Brazil), the Eastern Brazilian Pegmatite Province and related mineral resources. Geol. Soc. Lond. Spec. Publ. 350 (1), 25–51.
Pilet, S., Hernandez, J., Sylvester, P., Poujol, M., 2005. The metasomatic alternative for ocean island basalt chemical heterogeneity. Earth Planet. Sci. Lett. 236 (1–2), 148–166.
Peixoto, C., Heilbron, M., Diana Ragatky, D., Armstrong, R., Elton Dantas, E., Valeriano, C., Simonetti, A., 2017. Tectonic evolution of the Juvenile Tonian Serra da Prata magmatic arc in the Ribeira belt, SE Brazil: implications for early west Gondwana amalgamation. Precambrian Res. 302, 221–254.
Pilet, S., Baker, M.B., Stolper, E.M., 2008. Metasomatized lithosphere and the origin of alkaline lavas. Science 320 (5878), 916–919.
Rajesh, H.M., Santosh, M., 2004. Charnockitic magmatism in southern India. J. Earth Syst. Sci. 113, 565–585.
Rampone, E., Borghini, G., Basch, V., 2020. Melt migration and melt-rock reaction in the Alpine-Apennine peridotites: insights on mantle dynamics in extending lithosphere. Geosci. Front. 11 (1), 151–166.
Roden, M.F., Murthy, V.R., 1985. Mantle metasomatism. Annu. Rev. Earth Planet. Sci. 13 (1), 269–296.
Santiago, R., de Andrade Caxito, F., Neves, M.A., Dantas, E.L., de Medeiros Júnior, E.B., Queiroga, G.N., 2020. Two generations of mafic dyke swarms in the Southeastern Brazilian coast: reactivation of structural lineaments during the gravitational collapse of the Araçuaí-Ribeira Orogen (500 Ma) and West Gondwana breakup (140 Ma). Precambrian Res. 340, 105344.
Santiago, R., de Andrade Caxito, F., Pedrosa-Soares, A., Neves, M.A., Calegari, S.S., Lana, C., 2022. Detrital zircon U-Pb and Lu-Hf constraints on the age, provenance and tectonic setting of arc-related high-grade units of the transition zone of the Araçuaí and Ribeira orogens (SE Brazil). J. S. Am. Earth Sci. 116, 103861.
Schairer, J.F., Bowen, N.L., 1935. Preliminary report on equilibrium-relations between feldspathoids, alkali-feldspars, and silica. EOS Trans. Am. Geophys. Union 16 (1), 325–328.
Schannor, M., Lana, C., Mazoz, A., Narduzzi, F., Cutts, K., Fonseca, M., 2020. Paleoproterozoic sources for Cordilleran-type Neoproterozoic granitoids from the Araçuaí orogen (SE Brazil): constraints from Hf isotope zircon composition. Lithos 378, 105815.
Schmidt, M.W., Weidendorfer, D., 2018. Carbonatites in oceanic hotspots. Geology 46 (5), 435–438.
Serrano, P., Pedrosa-Soares, A., Medeiros-Junior, E., Fonte-Boa, T., Araujo, C., Dussin, I., Lana, C., 2018. A-type Medina batholith and post-collisional anatexis in the Araçuaí orogen (SE Brazil). Lithos 320, 515–536.
Soares, C., Queiroga, G., Pedrosa-Soares, A., Gouvêa, L.P., Valeriano, C.M., de Melo, M. G., Delicio, R., 2020. The Ediacaran Rio Doce magmatic arc in the Araçuaí-Ribeira boundary sector, Southeast Brazil: lithochemistry and isotopic (Sm-Nd and Sr) signatures. J. S. Am. Earth Sci. 104, 102880.
Söderlund, U., Patchett, P.J., Vervoort, J.D., Isachsen, C.E., 2004. The 176Lu decay constant determined by Lu-Hf and U-Pb isotope systematics of Precambrian mafic intrusions. Earth Planet. Sci. Lett. 219 (3–4), 311–324.
Sørensen, H., 1974. Alkaline Rocks.
Tedeschi, M., Novo, T., Pedrosa-Soares, A., Dussin, I., Tassinari, C., Silva, L.C., Heilbron, M., 2016. The Ediacaran Rio Doce magmatic arc revisited (Araçuaí-Ribeira orogenic system, SE Brazil). J. S. Am. Earth Sci. 68, 167–186.
Töpfner, C., 1987. Der Venda Nova Pluton im südlichen Espirito Santo, Brasilien; Geologische Kartierung des südöstlichen Teilgebietes sowie geochemisch-petrographische Bearbeitung des Charnockitischen Gesteinsgürtel. Unpublished master thesis. Ludwig-Maximilians-Universität München.
Tupinambá, M., Heilbron, M., Valeriano, C., Júnior, R.P., de Dios, F.B., Machado, N., Silva, L.G.D.E., de Almeida, J.C.H., 2012. Juvenile contribution of the Neoproterozoic Rio Negro Magmatic Arc (Ribeira Belt, Brazil): implications for Western Gondwana amalgamation. Gondwana Res. 21 (2–3), 422–438.
Upton, B.G., Thomas, J.E., 1980. The Tugtutoq younger giant dyke complex, South Greenland: fractional crystallization of transitional olivine basalt magma. J. Petrol. 21 (1), 167–198.
Valeriano, C.M., Mendes, J.C., Tupinambá, M., Bongiolo, E., Heilbron, M., Junho, M.D.C. B., 2016. Cambro-Ordovician post-collisional granites of the Ribeira belt, SE-Brazil: a case of terminal magmatism of a hot orogen. J. S. Am. Earth Sci. 68, 269–281.
Vauchez, A., Egydio-Silva, M., Babinski, M., Tommasi, A., Uhlein, A., Liu, D., 2007. Deformation of a pervasively molten middle crust: insights from the neoproterozoic Ribeira-Araçuaí orogen (SE Brazil). Terra Nova 19 (4), 278–286.
Vermeesch, P., 2018. IsoplotR: a free and open toolbox for geochronology. Geosci. Front. 9 (5), 1479–1493.
Vieira, V.S., Silva, M.A., Corrêa, T.R., Lopes, N.H.B., 2018. Mapa geológico do estado do Espírito Santo.

Wendlandt, R.F., 1981. Influence of CO2 on melting of model granulite facies assemblages: a model for the genesis of charnockites. Am. Mineral. 66 (11–12), 1164–1174.

Wiedemann, C.M., De Medeiros, S.R., Ludka, I.P., Mendes, J.C., Costa-de-Moura, J., 2002. Architecture of late orogenic plutons in the Araçuaí-Ribeira fold belt, Southeast Brazil. Gondwana Res. 5 (2), 381–399.

Willbold, M., Stracke, A., 2010. Formation of enriched mantle components by recycling of upper and lower continental crust. Chem. Geol. 276 (3–4), 188–197.